Title

Shifting groundwater fluxes in bedrock fractures: Evidence from stream water radon and water isotopes

Authors

Johnson, Keira
Christensen, John N
Gardner, W Payton
et al.

Publication Date

2024-05-01

DOI

10.1016/j.jhydrol.2024.131202

Peer reviewed

Journal Pre-proofs

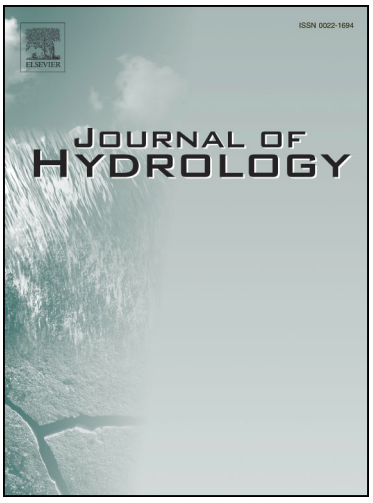

Research papers

Shifting groundwater fluxes in bedrock fractures: Evidence from stream water radon and water isotopes

Keira Johnson, John Christensen, W. Payton Gardner, Matthias Sprenger, Li Li, Kenneth H. Williams, Rosemary W.H. Carroll, Nicholas Thiros, Wendy Brown, Curtis Beutler, Alexander Newman, Pamela L. Sullivan

PII: S0022-1694(24)00597-3
DOI: https://doi.org/10.1016/j.jhydrol.2024.131202
Reference: HYDROL 131202

To appear in: *Journal of Hydrology*

Received Date: 13 July 2023
Revised Date: 8 March 2024
Accepted Date: 16 March 2024

Please cite this article as: Johnson, K., Christensen, J., Payton Gardner, W., Sprenger, M., Li, L., Williams, K.H., Carroll, R.W.H., Thiros, N., Brown, W., Beutler, C., Newman, A., Sullivan, P.L., Shifting groundwater fluxes in bedrock fractures: Evidence from stream water radon and water isotopes, *Journal of Hydrology* (2024), doi: https://doi.org/10.1016/j.jhydrol.2024.131202

Shifting groundwater fluxes in bedrock fractures: Evidence from stream water radon and water isotopes

Keira Johnson*, John Christensen, W. Payton Gardner, Matthias Sprenger, Li Li, Kenneth H. Williams, Rosemary W.H. Carroll, Nicholas Thiros, Wendy Brown, Curtis Beutler, Alexander Newman, Pamela L. Sullivan*

Keira Johnson, College of Earth, Ocean, and Atmospheric Sciences, Oregon State University.

ORCID: 0000-0003-0671-3901

John N. Christensen, Lawrence Berkeley National Laboratory, Berkeley, CA, USA

ORCID: 0000-0002-9533-5801

W. Payton Gardner, Dept. of Geosciences, University of Montana, MT, USA, ORCID: 0000-0003-0664-001X

Matthias Sprenger, Lawrence Berkeley National Laboratory, Berkeley, CA, USA, ORCID: 0000-0003-1221-2767

Li Li, Department of Civil and Environmental Engineering, Penn State University, ORCID: 0000-0002-1641-3710

Kenneth H. Williams

Lawrence Berkeley National Laboratory, Berkeley, CA USA

Rocky Mountain Biological Laboratory, Gothic, CO USA

ORCID; 0000-0002-3568-1155

Rosemary W.H. Carroll, Desert Research Institute, Reno, NV, USA.

ORCID. 0000-0002-9302-8074

Nicholas Thiros, Lawrence Berkeley National Laboratory, Berkeley, CA, USA, 0000-0002-1704-1031

Wendy S. Brown, The Rocky Mountain Biological Laboratory, Gothic, CO USA ORCID: 0000-0002-7237-1797

Curtis Beutler, Rocky Mountain Biological Laboratory, Gothic, CO USA

ORCID: 0000-0003-0740-3112

Alexander Newman, Rocky Mountain Biological Laboratory, Gothic, CO USA

ORCID: 0000-0002-1574-8754

Pamela L. Sullivan, College of Earth Ocean and Atmospheric Sciences, Oregon State University, ORCID: 0000-0001-8780-8501

*Corresponding Authors: Keira Johnson (johnkeir@oregonstate.edu) and Pamela L. Sullivan pamela.sullivan@oregonstate.edu

Keywords: groundwater surface water interactions, tracer hydrology, groundwater modeling, groundwater discharge, montane catchment

1.0 Introduction:

Streamflow derived from montane environments is important for downstream communities and ecosystem services but is vulnerable due to decreasing snowpack resulting from climate change (Viviroli et al., 2007; Mote et al., 2018; Viviroli et al., 2020). Earlier peak flows, smaller snowpacks, and higher evapotranspiration rates are predicted to decrease summer

flows (Stewart et al., 2005; Bavay et al., 2009; Ficklin et al., 2013; Azmat et al., 2016) leading to an increased reliance on groundwater (Kapnick and Hall, 2012; Somers et al., 2019). The relationship between groundwater and surface water (termed GW-SW interactions) is dominantly influenced by precipitation regime, vegetation, and geologic setting (Banks et al., 2011; Andermann et al., 2012; Safeeq et al., 2013; Carroll et al., 2018; Brooks et al., 2021). Especially of interest is summer precipitation (e.g., monsoon rains) which can contribute large amounts of water in the summer months (Shepard et al., 2002) and have the potential to buffer summer flows during low snowpack years (Carroll et al., 2020). Few studies have documented the impacts of monsoon rains on groundwater contribution in montane, snow dominated watersheds due to the remote nature of these catchments (Somers and McKenzie, 2020). Our understanding of GW-SW interactions can be enhanced with an improved understanding of the impacts of monsoon rains on groundwater contributions to summer flow, which is imperative for the future of water resources in montane environments.

GW-SW interactions are often difficult to quantify given the complex controls that geology exerts on spatial and temporal patterns of groundwater discharge (McClymont et al., 2012; Floriancic et al., 2018). Geologic features can play an important role in the locations and volume of groundwater discharge (Banks et al., 2009; Andermann et al., 2012). For example, in hard rock systems, groundwater predominantly flows through fractures due to their relatively higher permeability as compared to the surrounding matrix (Oxtobee and Novakowski, 2003). Groundwater in fractures can respond quickly to precipitation inputs (Flerchinger et al., 1993; Salve et al., 2012; Webb et al., 2017) rapidly recharging aquifers (Wittenberg et al., 2019) and discharging to streams (McDonnell et al., 1990). Alluvial deposits can also form in hard rock systems from long periods of sediment transport and deposition or glacial erosion. These deposits behave nearly opposite of fractured bedrock; they are characterized by high storage and have the potential to contribute large amounts of groundwater to summer stream flow over extended periods of time (Liu et al., 2004; Gordon et al., 2015; Käser and Hunkeler, 2016).

Hydrologic connectivity determines how different subsurface storage reservoirs contribute to surface water, and changes in hydrologic connectivity can be driven by changes in moisture conditions (Covino, 2017). Dynamic storage can be used as a proxy for hydrologic connectivity, where periods of higher dynamic storage indicate higher hydrologic connectivity (McIntosh et al., 2017; Dwivedi et al., 2018). Dynamic storage is part of overall catchment storage and defined as the variation in storage between wet and dry periods (Spence, 2007; Kirchner, 2009; Sayama et al., 2011; Dwivedi et al., 2018). Dynamic storage estimations have been leveraged to estimate subsurface storage (Sayama et al., 2011) and perform hydrograph separation (Dwivedi et al., 2018), and can be combined with other tracers leading to insights about flow path length and origin at the catchment scale. In montane environments, periods of high hydrologic connectivity typically occur during snowmelt, and recede throughout the summer (Jencso et al., 2010). However, in monsoon-impacted catchments, we expect that significant rainfall in the summer and fall months may temporarily increase hydrologic connectivity facilitating changes in GW-SW interactions. Additionally, we expect that the difference in storage capacity among geologic features in a catchment will cause them to respond variably to changes in moisture throughout the year, leading to shifts in dominant groundwater contributions throughout the summer (Käser and Hunkeler, 2016; Floriancic et al., 2018; Bush et al., 2023).

It is common to use geochemical and radioisotope tracers to quantify groundwater contribution to streamflow (Liu et al., 2004; Gardner et al., 2011; Gordon et al., 2015; Cowie et al., 2017; Beisner et al., 2018; Carroll et al., 2018). Radon (^{222}Rn; half-life 3.8 days) is an effective tracer because of its elevated concentration in groundwater from the continuous decay of uranium in rocks and soils (Webb et al., 2017). Compared to other geochemical tracers, ^{222}Rn helps identify areas of high groundwater contribution because it degasses upon interaction with the atmosphere. Thus, areas of high ^{222}Rn concentrations indicate localized groundwater flux into the stream. Radon has been used to assess groundwater contributions across a variety of environments including floodplains (Webb et al., 2017), urban rivers (Schubert et al., 2020), coastal streams (Peterson et al., 2010), mountain streams (Avery et al., 2018), and boreal lakes (Schmidt et al., 2010). Despite the wide range in geomorphic setting, few studies exist that use ^{222}Rn to identify groundwater contributions in montane environments (Gleeson et al., 2018). Radon can also be paired with non-degassing geochemical tracers to assess reach- or catchment-scale groundwater contribution (Genereux et al., 1993; Beisner et al., 2018; Gleeson et al., 2018; Cardenas et al., 2021). Stable water isotopes are a valuable tracer because they are conservative and are commonly used to assess groundwater contribution to montane streams (Fischer et al., 2015; Singh et al., 2016; Segura et al., 2019; Zuecco et al., 2018). Additionally, water isotopes vary with precipitation phase and season allowing for separation of streamflow into seasonal precipitation contributions (Allen et al., 2019a).

Significant advances in montane hydrodynamics could be achieved if the connectivity of geologic features to surface water could be more readily quantified. The aim of this paper is to understand how monsoon rains influence GW-SW interactions in bedrock fractures in a headwater stream of the Colorado River. We use ^{222}Rn and stable water isotopes to explore the seasonal variation of groundwater discharge in a Colorado River headwater stream (Figure 1b). To capture the influence of summer precipitation on groundwater discharge we collected roughly weekly, synoptic stream ^{222}Rn and water isotope samples across a stream reach of Coal Creek influenced by hillslope fractures. We focus on Coal Creek because the geologic setting gives rise to significant fracture networks (Figure 1c) and because of its potential for high monsoon efficiency (Carroll et al., 2020). Synoptic stream chemistry data were used to constrain a one-dimensional advective-dispersion model to estimate lateral groundwater discharge along the stream length throughout the summer.

2.0 Methods

2.1 Study Site

Coal Creek is a small (53 km^2), high-elevation, headwater tributary to the Upper Colorado Basin located on the traditional homelands of the Núu-agha-~~tuvu-pu~~ (Ute) peoples in the Ruby-Anthracite Range in the central Colorado Rocky Mountains. Coal Creek is located within the larger East River watershed (catchment area of 300 km^2), which is a designated Science Focus Area (Hubbard et al., 2018) by the Department of Energy and a watershed observatory within the Critical Zone Collaborative Network (CZCN) supported by the National Science Foundation. As such, the East River, including Coal Creek, hosts a diverse collection of hydro-biogeochemical measurements that provide an ideal setting for examining the controls of groundwater inputs under summer monsoon conditions. The watershed and its key tributary

drainages, including Coal Creek, are broadly representative of snow-dominated basins in the Rocky Mountains.

The Coal Creek in elevation from 2712 to 3668 meters. Coal Creek originates near Lake Irwin and enters the Slate River near the town of Crested Butte before joining the East River and eventually the Gunnison River. The watershed is seasonally snow-covered from November through June. The average temperature is 0.9˚C and it receives around 670 mm of precipitation each year, about 66% of which falls as snow (Carroll et al., 2018). The remaining precipitation falls during the summer monsoon season (July through September). Although monsoon rains comprise approximately 25% of the annual precipitation, they contribute only about 10% to the summer streamflow because the moisture is lost via evapotranspiration (Carroll et al., 2020; Sprenger et al., 2022). Vegetation in the basin is strongly aspect driven, with north facing aspects dominated by evergreen forest (65%) and south facing aspects dominated by deciduous (9%) and herbaceous (20%) vegetation. High elevation ridges are barren (3%) (Zhi et al., 2019). Discharge in Coal Creek is dominated by snowmelt, with average peak flow occurring in June. Flows recede throughout the summer and fall, with small peaks in flow due to monsoon events. Coal Creek reaches baseflow conditions by early September and they persist throughout the winter until the onset of snowmelt in April (Figure 2a).

The lower portion of the Coal Creek watershed is underlain predominately by sandstone (Upper Cretaceous Mesaverde Formation) with glacial till deposits occurring near the streambed. The upper portion of the watershed is underlain by mafic intrusive plutonic rock, emplaced during the Middle Paleocene. Areas of the upper north slope of the watershed are underlain by mudstone (Tertiary Wasatch Formation) (Figure 1b). Fractures have been mapped along the north hillslope in the upper watershed (Figure 1b). East of the mapped fractures is the contact between the upper basin intrusive plutonic rock and lower basin sandstone. This contact roughly bisects the Coal Creek watershed running northeast to southeast. Mapped along this contact zone, on either side of Coal Creek stream, is a dense spring network (Gaskill et al., 1991). Alluvial fans have been mapped at the confluence of tributaries with Coal Creek. These fans are Holocene age, poorly sorted material (Gaskill et al., 1991). Although many fans are present along the transect, our design only captures the alluvial fan associated with Elk Creek as our aim was primarily focused on the fracture zone compared to downstream behavior. Elk Creek is the only tributary that contributes significantly to streamflow generation along our study reach of Coal Creek throughout the summer.

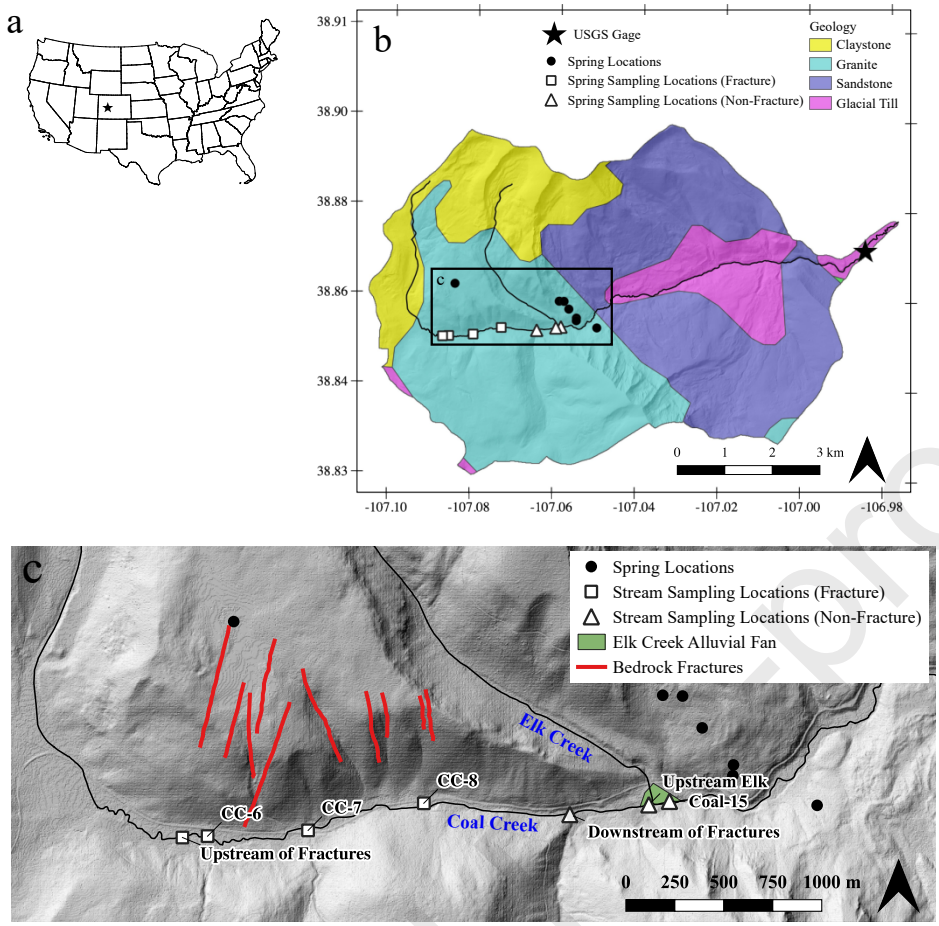

Figure 1: (a) Location of Coal Creek watershed within the United States. (b) Geologic map of Coal Creek (Horton et al., 2017) watershed showing stream sampling within fracture (white square) and non-fracture (white triangle) zone, spring sampling (black circles) locations, and Coal Creek USGS gage (black star). (c) Inset of sampling sites showing sampling locations relative to fractures (red lines) (Gaskill et al., 1991) and alluvial fan (green polygon).

2.2 *Field Sample Collection*

From June through October 2021 a total of 77 surface water samples and seven spring samples were collected for ^{222}Rn and water isotopes across eight stream sites and seven springs (Table 1). Stream water sampling locations were collected along a 2842 m length reach in the upper portion of Coal Creek watershed (Table S1). Sampling locations were selected to identify the influence of mapped bedrock fractures on stream chemistry and discharge. All samples were collected in the thalweg of the stream to ensure they were well mixed. Our study design focuses on bookending the known fracture zone along Coal Creek, with one site located just above the fractured hillslope (Upstream of Fractures, referred to as Upstream), three sampling locations located along the transect of the stream that runs along the base of the hillslope with the mapped fractures (CC-6, CC-7, CC-8; Figure 1B), and three samples below the fracture zone (Downstream of Fractures, referred to as Downstream; Upstream of Elk Creek, referred to as Upstream Elk; and Coal-15). We note that Upstream Elk and Coal-15 co-occur with the location of the alluvial fan at Elk Creek. Elk Creek was sampled three times throughout the summer (late

May, late July, early October) at its confluence with Coal Creek, although only one sample (late July) was analyzed for ^{222}Rn. To distinguish between the behavior of the bedrock fractures and non-fracture zones, the sites can be differentiated into fracture sites (< 2350 meters along reach, n=5) and non-fracture zone (> 2350 meters along reach, n=2). Over 80% of surface water samples were analyzed for both ^{222}Rn and water isotopes.

Of the seven springs, six were located on the south facing slope and one was located on the north facing slope. All but one of the springs were further east than the sampled stream reach. Each spring was sampled only once. Of the spring samples, four were analyzed for both ^{222}Rn and water isotopes.

2.2.1 Water Sampling

Locations in a stream with high ^{222}Rn concentrations indicate localized areas of groundwater discharge. ^{222}Rn is not affected by biological processes and is relatively inert, although is subject to physical loss and radioactive decay. Once groundwater enters the river, ^{222}Rn quickly dissipates due to degassing to the atmosphere (Schubert et al., 2020). Stream water was collected in 2L plastic bottles without headspace and spring water was collected in 500 mL plastic bottles (n=2) or 250 mL glass bottles (n=4) without headspace. Stream water was collected in large volume bottles to ensure accurate measurement and detection of ^{222}Rn due to the relatively low concentration of ^{222}Rn in stream water. Spring samples were collected in smaller bottles given the high concentration of ^{222}Rn in groundwater and were collected in different bottle types due to bottle availability at the time of sampling. Each spring was sampled only once, and one duplicate stream water sample was collected with three of the six synoptic events. All samples were collected using a Grainger surface water pump (Model IL200P, RULE, Rye Brook, NY) powered by a 12V battery. Due to the large volume of water we needed to collect for ^{22}Rn analysis, we designed a sampling scheme that pumped water from the thalweg to a 2L bottle onshore. The bottle was placed in a bucket with the tubing inside, filled, and capped underwater without headspace to minimize degassing of ^{222}Rn and the cap was sealed with Parafilm™. We sampled springs similarly by placing the pump in the pool at the spring head or as close to the spring head such that the pump was completely submerged. Samples were shipped in coolers overnight to Lawrence Berkeley National Lab for ^{222}Rn analysis.

Stream and spring water were also collected for stable water isotope analysis. Water samples were filtered through a 0.45-micron Nylon filter into a 2 mL glass vial with Septa caps taking care to eliminate headspace and refrigerated until analysis. We relied on water isotopes of precipitation collected about 10 km north-east of Coal Creek during the 2021 water year as end members to compare stream and spring water isotopic composition. Samples were collected approximately weekly, and snow (n=23) and rain (n=10) samples were aggregated to assess seasonal variability in precipitation (Table S2). Rain gauges were made to U.S. Weather Bureau specifications with a capacity of 27.9 cm x 2 mm. Gauges were situated in areas sheltered from winds, attempting to maintain at least two lengths of surrounding tree height to avoid turbulence. Mineral oil was used to limit evaporative effects.

2.2.2 Stream Discharge

We measured stream discharge five times between June 25th and August 30th at the sites: Upstream of Fractures, Downstream of Fractures, and Coal-15 (Table S3). Starting August 3rd, discharge measurements were moved downstream from Upstream of Fractures to CC-6 because of beaver activity that dammed the Upstream site. Discharge was measured using a SonTek FlowTracker Handheld Acoustic Doppler Velocimeter. Cross sections were selected based on characteristics of straight channel, minimal boulders on stream bed, and evenly distributed flow across the channel. Due to changes in flow depth, cross section location varied throughout the summer to achieve the most accurate measurements.

2.3 Isotope Sample Analysis

Concentrations of ^{222}Rn in the water samples were measured using a RAD7 instrument (mfd. by Durridge Co. Inc., Billerica MA). A closed loop system connected to the RAD7 (the RAD H20 for 2 L bottles - Durridge Co.) was used to sparge ^{222}Rn for quantification within the instrument. After 15-minutes of sparging, counting began for 15-minute periods. After the first four counting periods (or one hour) the internal air pump of the RAD 7 was turned off, and counting continued for at least 10 counting periods, or a total counting time of at least 2.5 hours. The average temperature of the water sample during the sparging process was measured using a thermo-couple electronic thermometer (Thermapen MK4, ThermoWorks, USA) held to the bottle with a Velcro strap. This temperature was used to calculate the partitioning of ^{222}Rn between the air-loop and the water sample. Between sample analyses, the entire system was purged for 15 minutes with the atmosphere to remove ^{222}Rn from the system and reduce internal humidity. Statistical pooling of the counting periods for individual analyses was conducted using Isoplot (Ludwig, 2012). Measured ^{222}Rn concentrations were corrected for radioactive decay to the time of sample collection (typically measurements were analyzed < 48 hrs. post sample collection). Average analytical uncertainty was 1.2 piC/L. ^{222}Rn concentrations are reported in Table 2 as pCi/L.

Hydrogen and oxygen isotope ratios of water were measured using an off-axis integrated cavity output spectrometer coupled to an autosampler interfaced with a heated injector block (Los Gatos Research, San Jose, USA). Average analytical uncertainty for hydrogen and oxygen isotopes are 0.05 and 0.14 per mil, respectively. Hydrogen and oxygen isotope ratios are reported in conventional δ notation relative to the Vienna Standard Mean Ocean Water.

2.4 Data Analysis

2.4.1 Discharge, Precipitation, and Evapotranspiration Metrics

Mean daily Coal Creek discharge was downloaded from the USGS gage 09111250. Daily precipitation and snow water equivalent (SWE) was downloaded from SNOTEL station 380 located on Mt. Crested Butte. Potential evapotranspiration (PET) was calculated using the Penman-Monteith equation using temperature, wind, dew point, and radiation data from the KCOCREST52 WunderGround weather station in Mt Crested Butte, Colorado. Both the SNOTEL and WunderGround stations are located outside the watershed but located at the approximate elevation of the Coal Creek watershed of 3149 m (3097 m and 2913 m, respectively).

2.4.2 Seasonal Origin Index

The Seasonal Origin Index (SOI) is a metric that expresses the isotope signature of the stream water relative to seasonal precipitation isotope cycles (Allen et al., 2019b). The SOI was calculated for each stream water sample using the following equation:

$$SOI = \begin{cases} \frac{\delta x - \delta_{annP}}{\delta_{summerP} - \delta_{annP}} & if\ \delta_x > \delta_{annP} \\ \frac{\delta x - \delta_{annP}}{\delta_{annP} - \delta_{winterP}} & if\ \delta_x < \delta_{annP} \end{cases}, \quad \text{(eq. 1)}$$

where δx is the $\delta^{18}O$ isotopic signature of stream water, and $\delta_{winterP}$, $\delta_{summerP}$, and δ_{annP} are the $\delta^{18}O$ isotopic signatures of volume-weighted winter, summer, annual precipitation at Coal Creek. The SOI is -1 when all the stream water is comprised of winter precipitation ($\delta_{winterP}$), +1 when all the stream water is comprised of summer precipitation ($\delta_{summerP}$), and 0 when the stream water isotopic composition is equivalent to the weighted average of all water year precipitation (δ_{annP}).

2.4.3 Estimation of Groundwater Discharge Volume

Groundwater discharge volume along the fracture zone was estimated for six different stream reaches throughout the summer (6/23-8/30) using StreamTran (Smerdon and Gardner, 2022), a Python-based, one-dimensional advective-dispersive transport model that uses coupled mass balance equations of ^{222}Rn concentration and discharge measurements along a transect to estimate lateral groundwater discharge into the stream. StreamTran does not account for increases in stream ^{222}Rn concentration due to hyporheic exchange. The mass balance equation representing discharge is given by:

$$\frac{dQ}{dx} = Pw - Ew + \frac{Q_T}{dx} + q_{gi}w - q_{go}w \quad \text{(eq.2)}$$

where Q ($m^3\ s^{-1}$) is stream discharge, x (m) is discretized distance downstream, P ($m\ s^{-1}$) is the precipitation rate, E ($m\ s^{-1}$) is the evaporation rate, Q_T ($m^3\ s^{-1}$) is tributary discharge, q_{gi} ($m\ s^{-1}$) is the groundwater discharge gain flux, q_{go} ($m\ s^{-1}$) is the groundwater loss flux, and w is the stream width in meters.

For 1d advective-dispersive transport of ^{222}Rn in the stream, including groundwater inflow, atmospheric gas exchange, and solute decay, the mass balance equation is given by:

$$\frac{dC}{dx} = \frac{d}{dx}\left(\frac{DA}{Q}\right)\left(\frac{dC}{dx}\right) + \frac{q_{gi}w}{Q}(C_{GW} - C) + \frac{Q_T}{dxQ}(C_T - C) - \frac{kw}{Q}(C - C_{ATM}) - \frac{A}{C}\lambda C \quad \text{(eq.3)}$$

where C ($mol\ m^{-3}$) is the stream concentration, D ($m^2\ s^{-1}$) is the longitudinal hydrodynamic dispersivity, A (m^2) is the stream cross-sectional area, C_{GW} ($mol\ m^{-3}$) is the local groundwater concentration, k ($m\ s^{-1}$) is the gas exchange velocity, C_{ATM} ($mol\ m^{-3}$) is the atmospheric equilibrium concentration of the tracer, λ (s^{-1}) is the decay coefficient, and C_T ($mol\ m^{-3}$) is the tributary concentration.

2.4.3.1 Solution technique and boundary conditions

Equations 2 and 3 are fully coupled and solved using a fully implicit, finite volume method based using *FiPy* (Guyer et al., 2009), a python finite volume solver library. Equation 2 and 3 are solved simultaneously to estimate groundwater gain and loss along the stream reach given measured discharge, stream geometry, tributary input, precipitation, evaporation, and ^{222}Rn concentration along the stream reach. The groundwater concentration of ^{222}Rn, ^{222}Rn gas exchange velocity, and ^{222}Rn decay coefficient are required estimated parameters. The coupled equations are optimized using a Marquart-Levenberg optimization routine to minimize the chi squared residual between the observed and modeled ^{222}Rn and discharge stream measurements. From these optimized equations, groundwater discharge is estimated along the transect at *n* equally spaced intervals, where *n* is equal to the number of samples.

The stream is discretized into 10000 equally spaced approximately ⅓ meter grids from upstream to downstream. Model unit length varied between sampling date 08/30/21 and other dates because samples from 08/30/21 began further downstream due to new construction of a beaver dam at the Upstream sampling location. Constant discharge and concentration (Dirichlet) boundary conditions are set at the upstream end of the model and set to the measured concentration and discharge at the most upstream site for a given sampling event. Constant discharge (Dirichlet) and constant concentration gradient (Neumann) boundary conditions are set at the downstream end of the model.

2.4.3.2 Parameterization

The model was parameterized to represent site conditions at the time of synoptic sampling (Table 1). Atmospheric equilibrium concentration of ^{222}Rn was set to zero. The ^{222}Rn decay coefficient was set to 3.82 d^{-1} (Cook and Herczeg, 2000). The fully implicit finite volume technique used controls the dispersive flux in the solution even when set to zero. Therefore, longitudinal hydrodynamic dispersivity was set to zero, which means that numerical dispersion of the grid cell spacing (~1/3 m) controls the dispersive flux (Beisner et al., 2018). Stream width and depth were measured each time discharge was measured (SI Table 1, SI Text 1) and linearly interpolated along the stream reach.

Initial ^{222}Rn gas exchange velocities were calculated for each sampling event using estimated stream geometry and flow characteristics and were assumed to be constant for the length of the reach (SI Table 2). Groundwater ^{222}Rn concentration was measured from six springs across the watershed. Calculated gas exchange velocities based on equations from Raymond et al., (2012) and measured ^{222}Rn concentrations lead to underestimation of discharge and overestimation and ill-fitting of measured ^{222}Rn concentrations (Text S3; Figures S2 and S3), which is not surprising given that gas exchange velocity and groundwater ^{222}Rn concentrations are highly variable (Ulseth et al., 2019; Mullinger et al., 2009). Therefore, we used Monte Carlo simulations to estimate a range of gas exchange velocities and groundwater ^{222}Rn concentrations. Gas exchange velocity is highly dependent on-stream turbulence. For high-energy, montane streams, the accuracy of empirical equations for estimating gas exchange velocity often diminishes. For streams with slopes similar to Coal Creek (0.029 m m^{-1}), gas exchange velocities have been observed between 1 and 100 m d^{-1} (Ulseth et al., 2019). Monte Carlo simulations were run for each modeled sampling event using gas exchange velocities between 10 and 105 m d^{-1} ($\leq$ 10 times estimated gas exchange velocity using empirical equations (SI Text 2)) and groundwater ^{222}Rn concentrations between 100 and 600 piC L^{-1} (approximate minimum and

maximum measured spring concentrations; Table 1). A total of 3,000 Monte Carlo simulations per modeled synoptic event were run to estimate the gas exchange velocity and groundwater ^{222}Rn concentration for each synoptic event. Model fit was evaluated using the Akaike Information Criterion (AIC). AIC is an estimation of prediction error, generally used to compare models and determine which is the best fit for the data (Bozdogon, 1987). Here, low AIC values indicate better fit between measured and modeled discharge and ^{222}Rn concentrations. To represent a range of conditions which may give optimal model performance, we evaluated groundwater ^{222}Rn concentrations and gas exchange velocities from model runs within the top 5% of AIC values (150 runs for each synoptic event). The median values of groundwater ^{222}Rn concentration and gas exchange velocity from the top 5% simulation runs were used to parameterize the StreamTran model. Pairings of the minimum groundwater ^{222}Rn concentration and minimum gas exchange velocity, and the maximum groundwater ^{222}Rn concentration and maximum gas exchange velocity, from the top 5% best models were used to characterize uncertainty around the MC estimated groundwater flux.

Table 1: Model input parameters.

Parameter	Definition	Value	Note
P	Precipitation (ms^{-1})	0	Field conditions
E	Evaporation (ms^{-1})	Table S5	Estimated using Penman-Monteith
w	Width (m)	Table S4	Stream discharge measurements
d	Depth (m)	Table S4	Stream discharge measurements
A	Cross Sectional Area (m^2)	w*d	Stream discharge measurements
D	Dispersivity $(m^2s^-)^1$	0	Beisner et al. (2018)
$k^\dagger$	gas exchange velocity (ms^{-1})	Table 3	Estimated using MC simulation

Parameter	Definition	Value	Note
P	Precipitation (ms^{-1})	0	Field conditions
E	Evaporation (ms^{-1})	Table S5	Estimated using Penman-Monteith
w	Width (m)	Table S4	Stream discharge measurements
d	Depth (m)	Table S4	Stream discharge measurements
A	Cross Sectional Area (m^2)	w*d	Stream discharge measurements
λ	Rn decay coefficient (s^{-1})	$4.43x10^{-5}$	Cook and Herczeg (2000)
C_{atm}	Atmospheric ^{222}Rn concentrations (piC/L)	0	Field conditions
C_{gw}†	Groundwater ^{222}Rn concentrations	Table 3	Estimated using MC simulation
C_{tr}	^{222}Rn concentration in Elk Creek (piC/L)	2.1	Field conditions, measured on July 27, 2021

† indicates parameters that varied during optimization routine

2.4.3.3 Discharge and stream geometry relationships

Discharge along the modeled stream reach is a required input for parameterization of StreamTran. Discharge was measured five times throughout the summer at Upstream/CC6,

Downstream, and Coal-15. Upstream and CC6 are combined into one site because beginning August 3rd measurements had to be moved downstream from Upstream to CC6 due to construction of a new beaver dam. These two sites are 161 m apart. Since stream discharge is responsive to monsoon rains, using measured discharge close to the sampling date is not sufficient. Thus, linear regressions between each measured site and the USGS gage data were performed to estimate discharge along the stream reach throughout the summer (Figure S1).

Width and depth were measured with discharge and are also required inputs along the stream reach. However, these parameters are responsive to changes in discharge and thus to precipitation inputs from monsoon rains. Width and depth were regressed against measured discharge (Figure S1), and those relationships were used to estimate width and depth from modeled discharge. Modeled discharge, width, and depth were used as inputs for each transect run in StreamTran (Table S5).

2.4.4 Estimation of dynamic storage

We estimated the change in dynamic storage of Coal Creek over the course of the summer using a water balance analysis. The change in dynamic storage (*dS*) was calculated as follows:

$$dS(t) = \sum_{t=1}^{T}(P(t) - Q(t) - ET(t)) \quad \text{(eq.4)}$$

where *t* is time in days (in this study t=1 on June 1, 2021), *P* is precipitation (mm), *Q* is stream water discharge (mm), and *ET* is evapotranspiration (mm). Actual ET measurements are not available for Coal Creek; we use PET calculated from the Penman Monteith equation in our calculations of *dS*. Coal Creek is a well-watered system and meets most of the assumptions required for Penman Monteith. The *dS* was calculated at a daily time stamp between June 1 and September 30. This water budget does not account for interbasin groundwater flow nor overland flow out of the catchment that is not routed into the stream. Although this is a simplification of the water budget, it represents the dominant processes that control water fluxes in montane catchments (Ryken et al., 2021). Uncertainty around *dS* was estimated assuming a 10% error in precipitation measurement (Larson, 1974; Ehsani and Behrangi, 2022), a 20% error in PET relative to AET (Hua et al., 2020; Westerhoff, 2015; Klingston et al., 2009), and a 13% error in stream water discharge calculated as the average percent difference between measured and gage-estimated discharge values for Coal Creek.

3.0 Results

3.1 Hydro-climatology of Coal Creek

In Coal Creek, the 2021 water year was overall drier than average, receiving only 523 mm of precipitation, compared to the average 658 mm. However, the precipitation deficit was confined predominantly to winter (October 1 – March 31) and spring (April 1-June 29), where only 290 mm and 88 mm of precipitation fell, compared to the average 387 mm and 126 mm, respectively. The total amount of rain during the summer (June 30-September 30) was equivalent to the average (145 mm). The snow drought of 2021 led to 62% lower than average peak flows (6.05 $m^3\ s^{-1}$) and 57% lower than average summer base flows (0.095 $m^3\ s^{-1}$; defined as the 10th

percentile flow between July 1 and September 30). Precipitation events during the summer of 2021 were generally concentrated between late June and July, with occasional precipitation events occurring through the rest of the summer (Figure 2b).

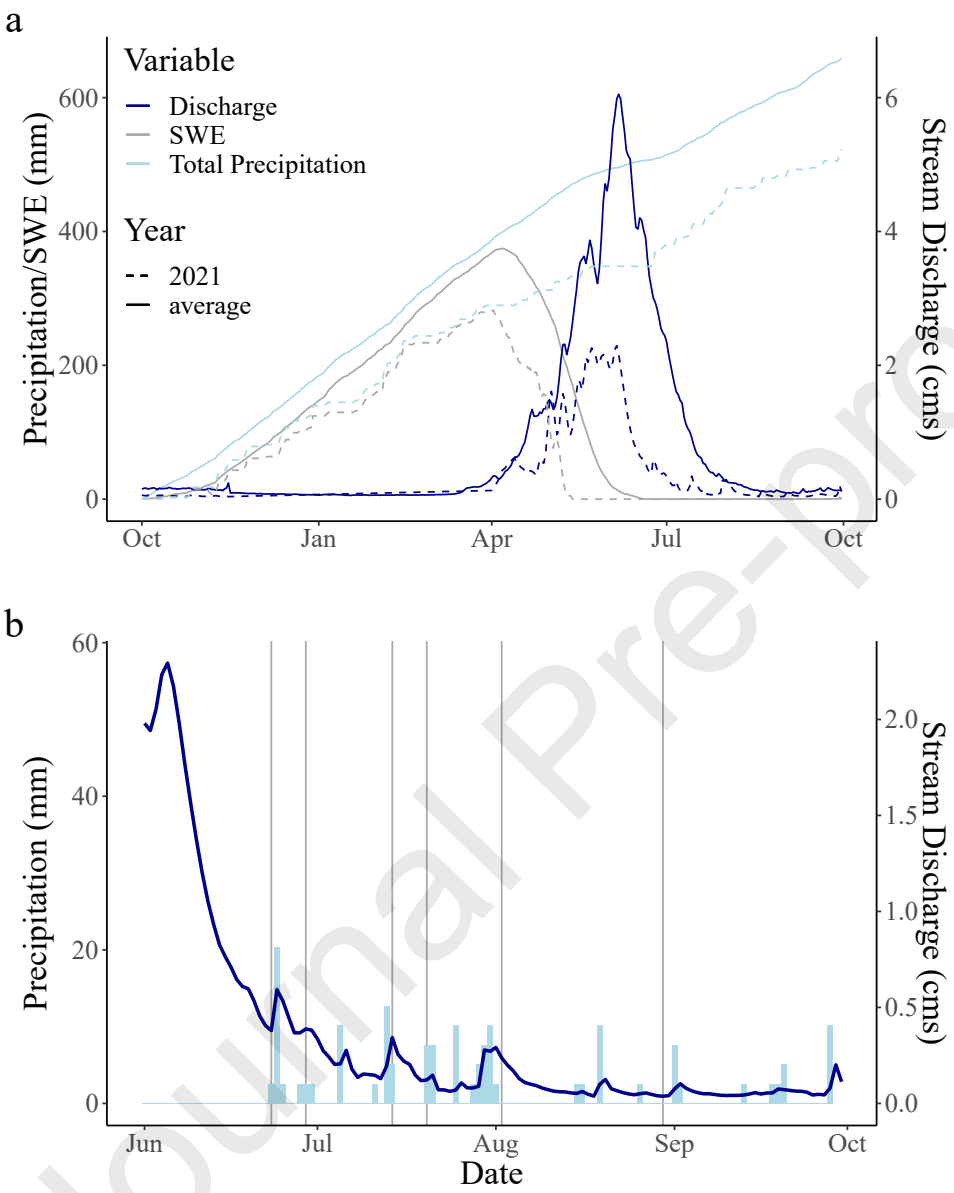

Figure 2: (a) Average water year precipitation accumulation (left-hand axis), snow water equivalent (SWE, left-hand axis), and stream discharge (right-hand axis) in Coal Creek. Dashed lines, but same color coding, show the respective curves for the 2021 water year. (b) Precipitation events and stream discharge (same color scheme as above) during summer sampling period (June 1 - September 30, 2021). Gray vertical lines indicate sampling dates included in the model.

3.2 Evaluating stream response to monsoon rains through synoptic stream chemistry sampling

3.2.1 Radon Samples

Stream water ^{222}Rn concentrations ranged from 2 to 20 piC/L, while spring water samples varied from 183 to 651 piC/L. The highest stream ^{222}Rn was measured at Upstream Elk and the lowest was measured at Downstream (Figure 3). ^{222}Rn was least variable at Upstream of Fractures (deviation from mean (%Dev) < 20%), moderately variable at CC6, CC8, and Downstream of Fractures (20% < %Dev < 30%), and highly variable at CC7, Upstream of Elk, and Coal-15 (%Dev > 30%) (Table 1, Figure 3).

Table 2: Sites, times sampled, stream meter, and mean and deviation from mean (standard deviation/mean) of ^{222}Rn, $\delta^{18}O$ and $\delta^{2}H$ water isotope measurements.

Site	Class	Times Sampled	Stream Meter	^{222}Rn Mean (piCL^{-1})	^{222}Rn Dev. from Mean (%)	$\delta^{18}O$ Mean (‰)	$\delta^{18}O$ Dev from Mean (%)	$\delta^{2}H$ Mean (‰)	$\delta^{2}H$ Dev from Mean (%)
Upstream	fracture	7†	11956	3	16	-16.1	1.86	-118.5	2.5
CC6	fracture	11†	11795	4	26	-15.8	5.70	-116.0	5.5
CC7	fracture	12†	11155	4	43	-15.6	4.49	-115.0	4.6
CC8	fracture	13†	10419	5	27	-15.6	4.49	-114.7	4.6
Downstream	fracture	9†	9632	2	25	-15.8	3.80	-116.4	3.4
Upstream Elk	non-fracture	9†	9221	12	46	-15.5	3.87	-114.2	4.0
Elk Creek	non-fracture	3†	9196	2	NA	-16.7	3.17	-122.3	3.82

Coal15	non-fracture	13†	9108	7	33	-15.6	3.21	-116.6	3.5
Spring 1‡	spring	1	NA	208	NA	NA	NA	NA	NA
Spring 2	spring	1	NA	619	NA	-17.2	NA	-125.6	NA
Spring 3‡	spring	1	NA	651	NA	NA	NA	NA	NA
Spring 4	spring	1	NA	NA	NA	-17.1	NA	-125.1	NA
Spring 5	spring	1	NA	608	NA	-16.6	NA	-125.2	NA
Spring 6‡	spring	1	NA	265	NA	-17.5	NA	-128.3	NA
Spring 7‡	spring	1	NA	183	NA	-17.1	NA	-123.8	NA

426 † Number of samples analyzed for isotope data; ^{222}Rn analysis was conducted two fewer times than the listed value.

427 ‡ Indicates ^{222}Rn and water isotope samples were collected on different days and that ^{222}Rn concentrations were
428 collected in 250 mL glass vials. Unmarked spring samples were collected in 500 mL plastic bottles.

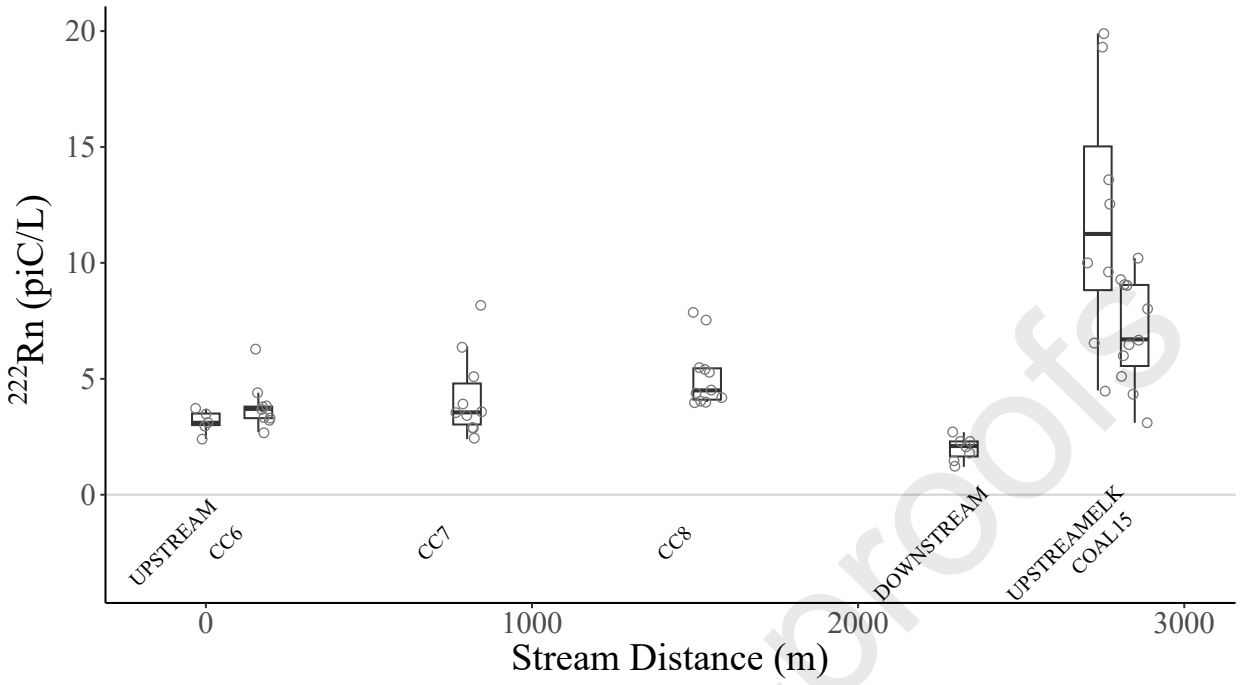

429

430 Figure 3. ^{222}Rn concentrations at surface water locations with distance downstream, not including Elk Creek.
431 Lower and upper lines of boxplot box are quartile 1 and 3, respectively. The middle line is the median. Vertical lines
432 indicate minimum and maximum, if less than +/- 1.5*interquartile range (IQR). Points outside +/- 1.5*IQR are
433 considered outliers and are plotted above/below vertical lines. Open points show all samples collected on a given
434 date.

435 Increasing or decreasing patterns of ^{222}Rn were not temporally consistent at all sites
436 (Figure 4a). In general, fracture zone sites showed a decreasing trend in ^{222}Rn concentration at
437 the beginning of the summer before flattening out in July, and then increased again in late
438 summer/early fall. Unlike the fracture zone sites, ^{222}Rn concentrations at Coal-15 were low in
439 June and increased throughout the summer before decreasing again at the end of summer. ^{222}Rn
440 concentrations at Upstream Elk were also high during summer and declined at the end of the
441 summer. Across all sites, peaks in ^{222}Rn were observed in mid-July, and non-fractured zone sites
442 there was an additional peak observed in mid-August peak. In general, peaks coincided with dry
443 periods while lower ^{222}Rn concentrations coincided with periods of time with more precipitation.

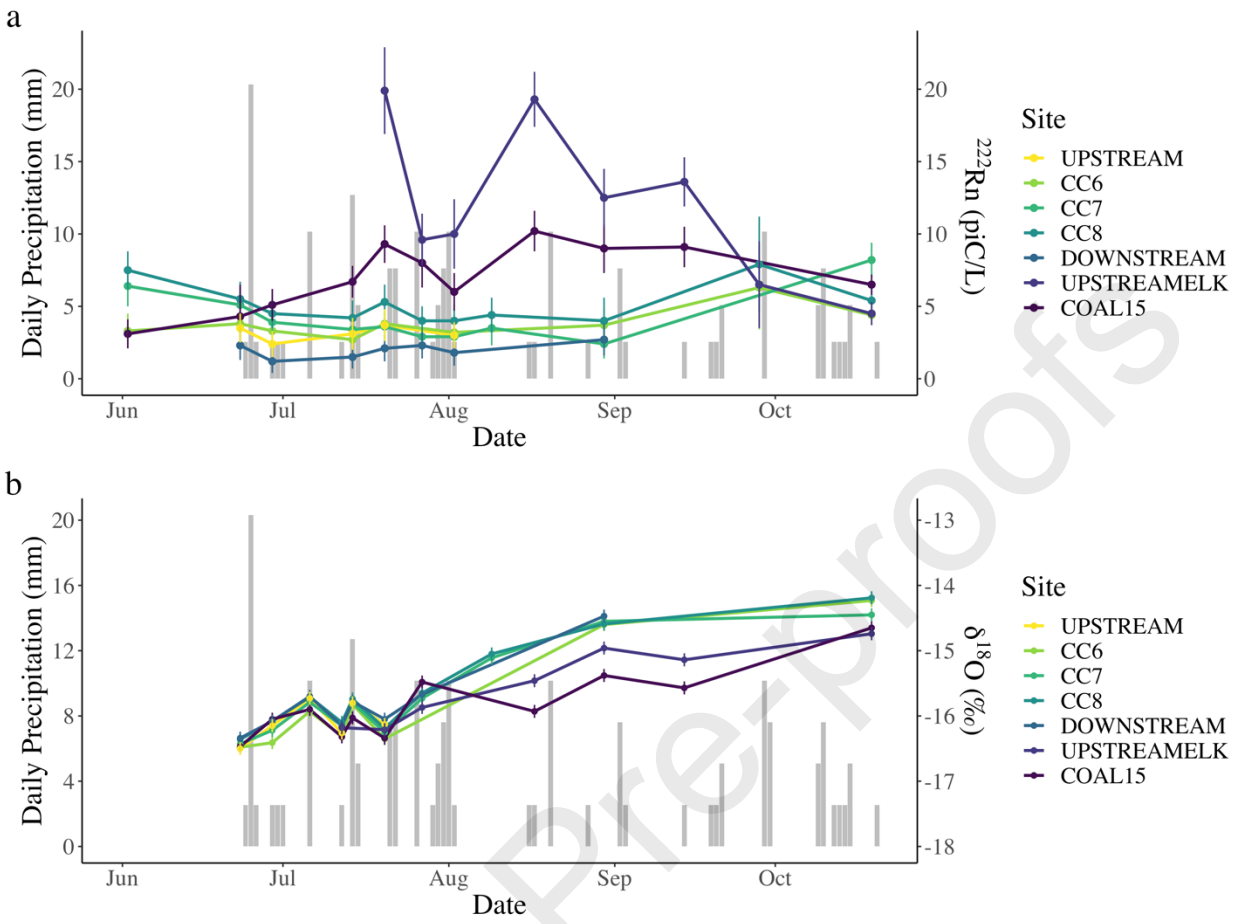

Figure 4. (a) ^{222}Rn concentrations and (b) $\delta^{18}O$ values and the analysis uncertainty (vertical lines) at sites (colored lines) as compared to the daily precipitation at Coal Creek (gray bars).

3.2.2 Water Isotope Samples

Stream water $\delta^{18}O$ values ranged from -16.5 to -14.2 ‰, while spring water samples were consistently more depleted than stream water and varied from -17.54 to -16.56 ‰ (Figure 5). Precipitation $\delta^{18}O$ values ranged from -3.83 to -26.64 ‰ (δ_{annP} = -14.67 ‰); summer rain events (2021 $\delta_{summerP}$ = -6.95 ‰) were generally more enriched than winter snow events (2021 $\delta_{winterP}$ = -19.56 ‰). Compared to ^{222}Rn concentrations, there was less distinct spatial variation in stream $\delta^{18}O$ values.

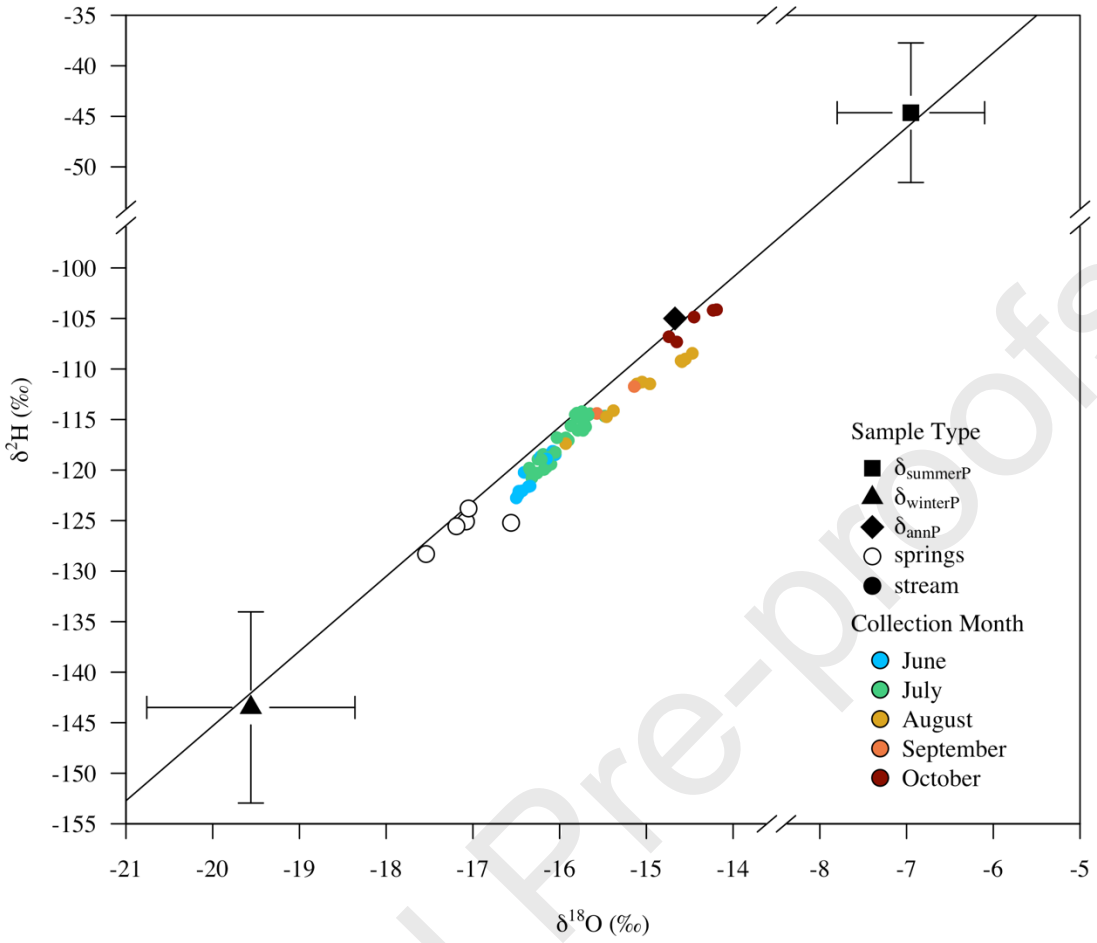

454

455 Figure 5: Dual isotope plots showing $\delta_{winterP}$ (weighted average snow, triangle), $\delta_{summerP}$ (weighted average
456 rain, square), and δ_{annP} (weighted average annual precipitation, diamond), spring samples (open circles),
457 stream samples (colored circles), and the local meteoric water line (LMWL) (black line) (developed by
458 Carroll et al., 2018). Error bars around precipitation end members indicate weighted standard errors.
459 Colors indicate sample collection month.

460 There was a strong temporal variation in stream water isotope composition with more
461 depleted values measured at the beginning of summer and more enriched samples measured at
462 the end of summer (Figure 5). In general, $\delta^{18}O$ enrichment was more pronounced in fracture zone
463 sites than the non-fractured zone sites, with fracture zone sites becoming more enriched later in
464 the summer in comparison to non-fractured zone sites. Across the entire stream transect in July,
465 variability in stream $\delta^{18}O$ values were observed, where samples collected following precipitation
466 events (e.g., 07/06, 07/14, and 07/27) had more enriched isotopic compositions and samples
467 collected during drier periods (i.e., 07/12 and 07/20) had more depleted isotopic compositions
468 (Figure 4b). This suggests that during July, Coal Creek may be responding quickly to
469 precipitation events, but this stream response was not observed in sampling events outside of
470 July.

The patterns present in the temporal variation of $\delta^{18}O$ (Figure 4b) are reflected in the Seasonal Origin Index (SOI) (Figure 6). The SOI estimates the proportion of water in the stream originating as winter (snow) vs summer (rain) precipitation (Figure 5). Within Coal Creek, the SOI of most stream water samples were negative, with only late season mean SOI value falling slightly above zero. SOI ranged from -0.37 to 0.06, with the most negative values observed during the earliest sampling event and the positive values observed during the latest sampling period. The variability in stream $\delta^{18}O$ composition observed in Figure 4b is also present in Figure 6 from dates 07/06 through 07/27. This is followed by an increase in SOI, indicating that at the beginning of the summer, stream water origin is more snow-dominated and becomes less snow-dominated throughout the summer.

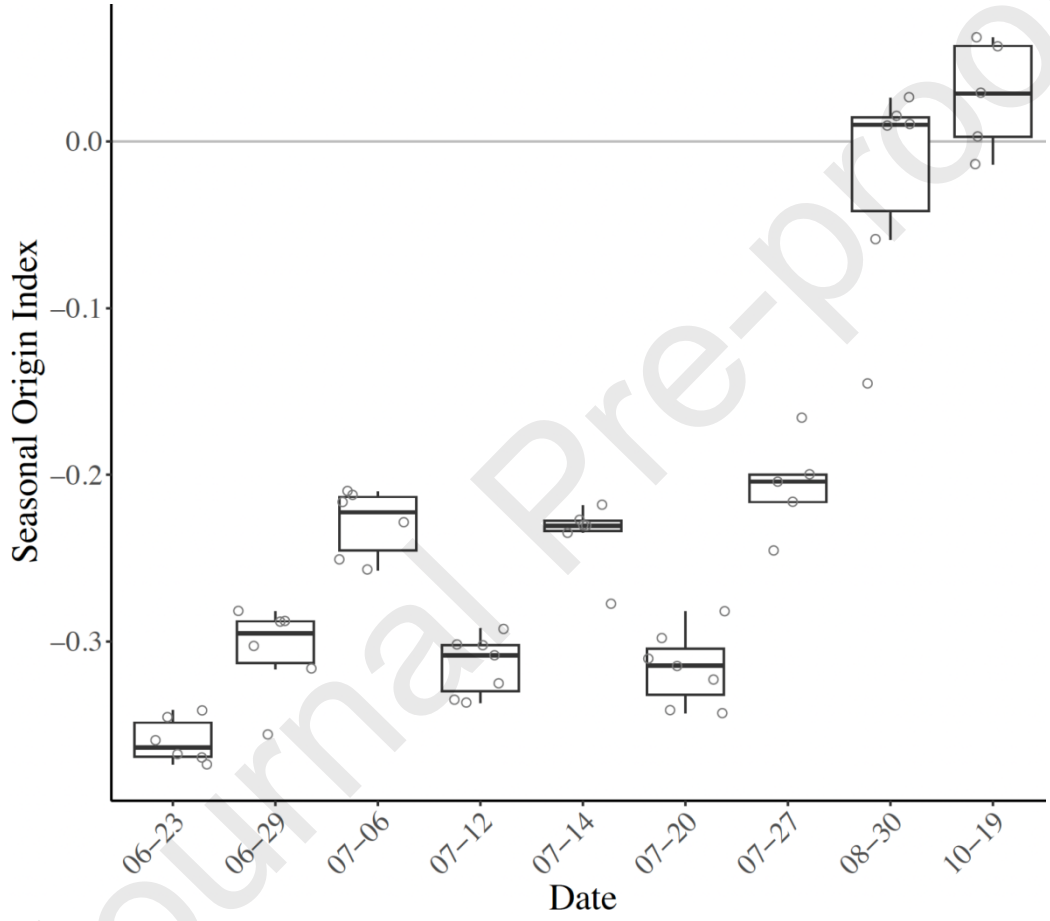

Figure 6: Seasonal origin index (SOI) for stream samples at Coal Creek. Lower and upper lines of the boxplot box are quartile 1 and 3, respectively. The middle line is the median. Vertical lines indicate minimum and maximum, if less than +/- 1.5*IQR. Points outside +/- 1.5*IQR are considered outliers. Open points show all samples collected on a given date. Horizontal gray line shows SOI of 0.

3.3 Model Parameterization and Performance

We used the StreamTran model to estimate groundwater flux into the stream between Upstream/CC6 and Coal-15 across six different dates throughout the summer. Monte Carlo simulations were used to estimate the gas exchange velocity and groundwater ^{222}Rn concentration for each synoptic event. Values used to parameterize each synoptic event were the

median of the top 5% best (lowest AIC) MC simulations (Table 3). Median groundwater ^{222}Rn concentrations ranged from 130 to 256.5 and median gas exchange velocities ranged from 48.5 to 90. Model performance varied across modeled events, with the best performing model representing stream conditions on 07/14 (AIC = 48.08) and the worst performing model representing stream conditions on 07/20 (AIC = 73.14). Both modeled stream discharge and stream ^{222}Rn concentrations generally agreed with measured values, with slight overprediction of stream discharge during 06/23, 06/29, and 07/14, and slight overprediction of stream ^{222}Rn concentrations during 07/20 and 08/02.

Table 3: Median output from top 5% Monte Carlo simulation runs for groundwater ^{222}Rn concentrations and gas exchange velocity (GEV) for the six model dates. Final model AIC is shown as well.

Date	Median ^{222}Rn (piC/L)	Median GEV (m/d)	Final Model AIC
06/23	139.5	90.0	59.03
06/29	130.0	86.5	54.98
07/14	137.0	84.0	48.08
07/20	256.5	48.5	73.14
08/02	188.5	73.0	65.73
08/30	245.5	77.5	60.08

501

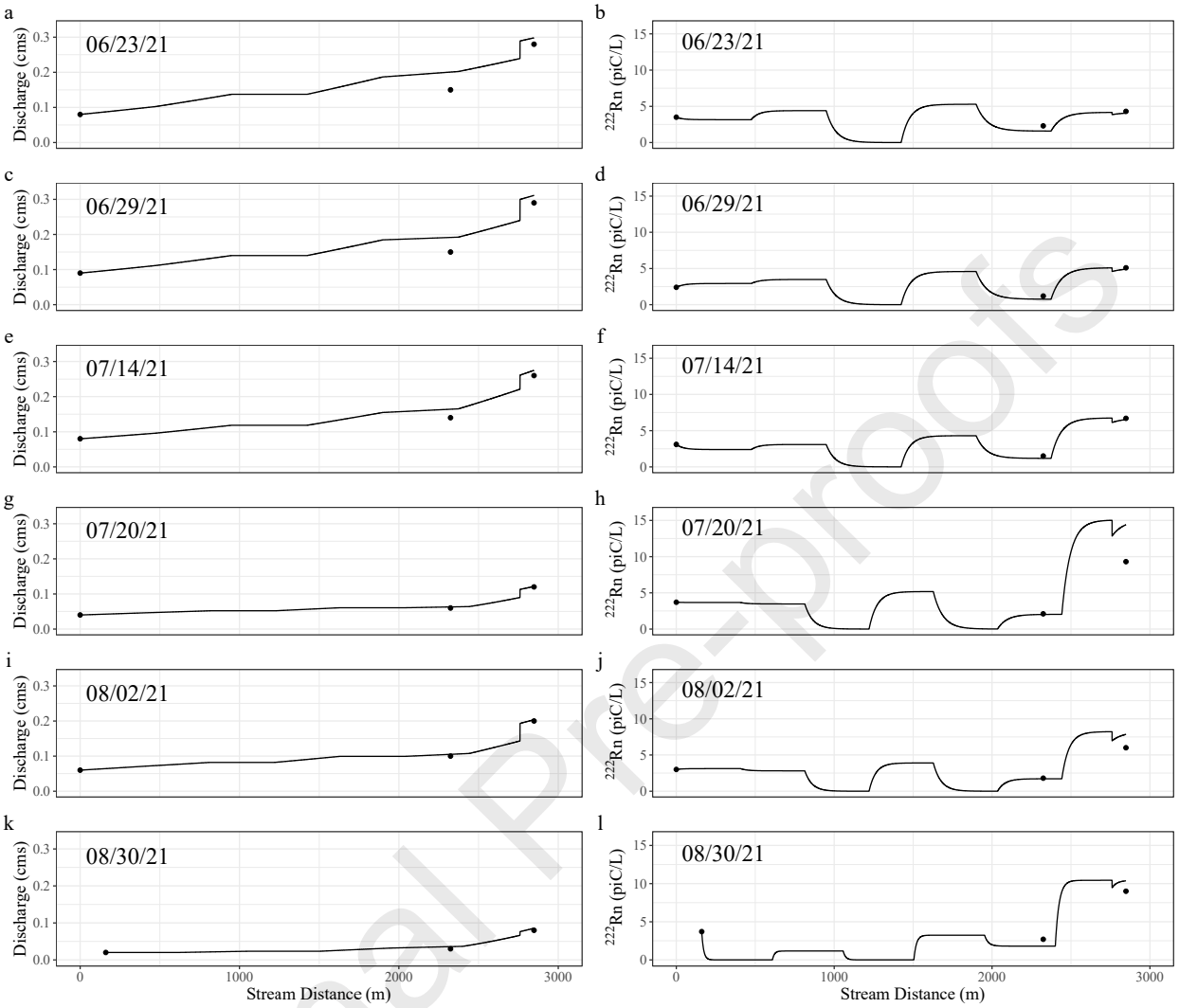

502

503 Figure 7: Stream discharge (a, c, e, g, i, k) and stream ^{222}Rn concentration (b, d, f, h, j, l) measurements (points)
504 compared to StreamTran modeled values (line) along the stream reach.

505 *3.4 Estimation of lateral groundwater flux through space and time*

506 By evaluating the groundwater flux (Figure 8) we can quantitatively evaluate how
507 groundwater discharge varied in space and time. There were two distinct spikes in GW flux
508 along the fractured zone and consistently high GW flux in the non-fractured zone (Figure 8). We
509 categorized two different temporal behaviors: early summer (06/23-07/14) and late summer
510 (07/20-08/30). In general, during early summer, groundwater contributions between both the
511 fractured and non-fractured zones were similar. The highest flux from the fractures and lowest
512 flux from the non-fractured occurred on 06/23 and the lowest flux from the fractures and highest
513 flux from the non-fractured zone occurred on 07/14. There was similar spread between all three
514 early summer sampling dates across all three areas of groundwater contribution. In contrast,
515 during late summer, groundwater contribution from the fractured zone was lower than that from

the non-fractured zone fan, and contribution from the fractured zone was more variable compared to the non-fractured zone contribution.

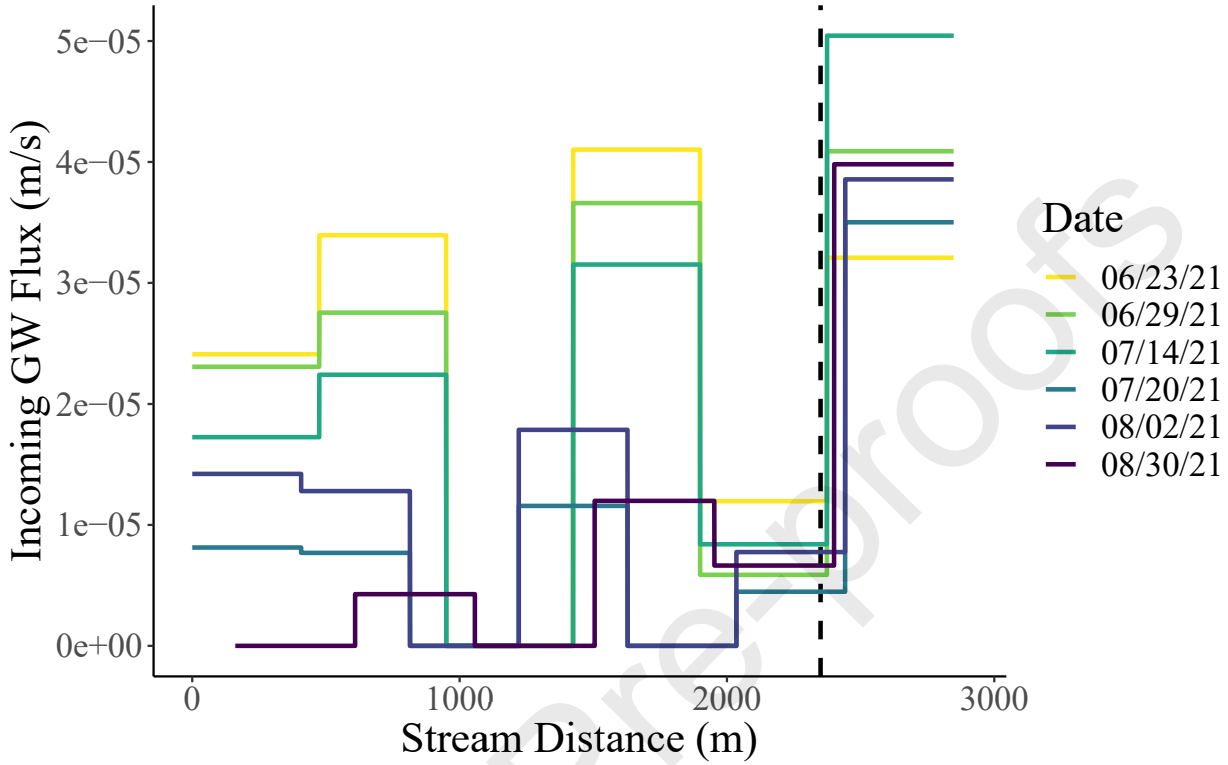

Figure 8: Groundwater flux along stream reach for six different modeled dates (colored lines). Flux represents a constant groundwater flow into the stream along each discretized section. Dashed line indicates the transition from the fracture zone to non-fractured fan.

To convert to groundwater discharge, flux was multiplied by the average width of the stream and 0.3 meters, which is the length of one discretized model unit. Cumulative groundwater discharge shows a similar divide between early and late season sampling events (Figure 9a). Early summer events show a larger absolute groundwater discharge and steeper and steadier slope in groundwater discharge over the stream transect than late season events. Late season events show a flatter slope in the upper portion of the stream transect, indicating less groundwater discharge across the fracture zone, with a similar slope when compared to early season sites along the non-fractured zone.

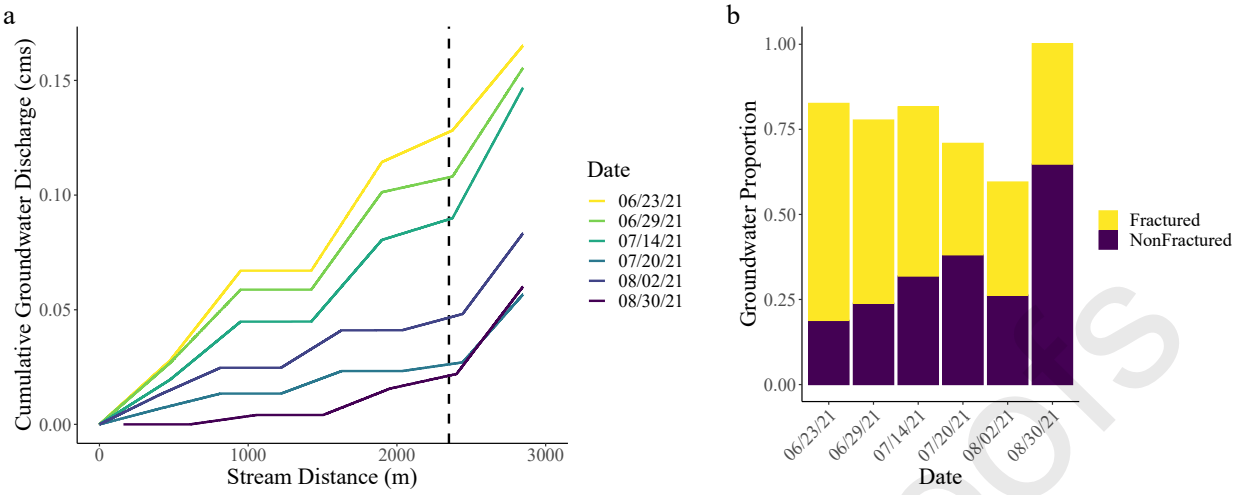

Figure 9: (a) Cumulative groundwater discharge ($m^3 s^{-1}$) along the stream length of Coal Creek for six different modeled dates (colored lines). This assumes that groundwater discharge above the most-upstream-sampled location was zero. Dashed lines indicate transitions from fracture to non-fractured zone (2350 m). (b) The proportion of increase in flow between Upstream/CC6 and Coal-15 attributed to groundwater for the six different modeled dates colored according to the amount contributed from the fracture zone (< 2350 m, yellow) and the non-fractured zone (< 2350 m, deep purple).

Across the six dates, the proportion of groundwater contribution to the modeled reach ranged from 60% on August 2 to 95% on August 30 (Figure 9b). Water from the fracture zone contributed between 35% and 77% of total groundwater with the highest proportional contribution early in the summer. Water from the non-fractured zone contributed between 23% and 65% of total groundwater with the highest proportional contribution later in the summer (Figure 9b). Fracture zone contributions declined both volumetrically and proportionally throughout the summer whereas non-fractured zone volumetric contributions stayed relatively constant and increased their proportion.

3.5 Relating dynamic storage to SOI and groundwater discharge

We evaluated how catchment storage changed over the course of the summer using changes in daily dynamic storage. Dynamic storage was highest during the beginning of the summer and lowest at the end of the summer (Figure 10a). Over the course of the sampling period used for modeling (6/23/21 to 8/30/21) dynamic storage declined by 176 mm, indicating significant draining of the dynamic storage zone throughout the summer. We evaluated the relationship between dynamic storage and SOI, cumulative groundwater discharge, and the ratio of fractured zone to non-fractured zone groundwater discharge across the six modeled sampled dates (Figure 10). We found significant relationships between dynamic storage and all three parameters, indicating that periods of higher connectivity (i.e., higher dynamic storage) are associated with more snow dominated streamflow and more groundwater discharge, specifically originating from the fractured zone, into Coal Creek.

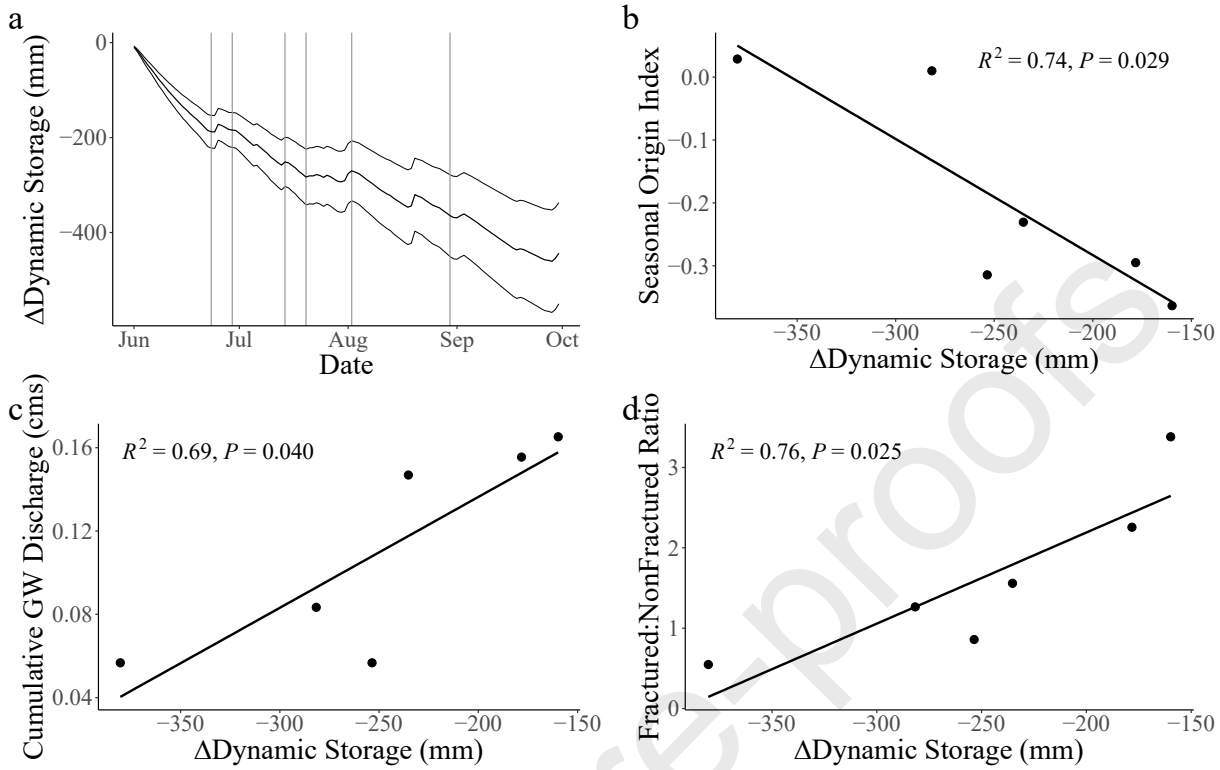

Figure 10: (a) Change in dynamic storage throughout the summer. Modeled sample dates are shown as vertical lines and uncertainty around the calculated dynamic storage value is shaded grey. Panels b-d show the relationships between change in dynamic storage and (b) seasonal origin index, (c) mean groundwater flux, and (d) the ratio of fractured zone to non-fractured zone groundwater discharge. R^2 and p-values for each relationship are shown in the respective panel. All relationships are significant at the 0.05 level.

4.0 Discussion

Changing subsurface connectivity due to variable moisture conditions is well documented across diverse watersheds (Blume and van Meerveld, 2015; Covino, 2017). Hydrologic connectivity describes how deep and shallow groundwater link to surface water, where in highly connected watersheds streamflow is typically older and groundwater is typically more important for streamflow generation (Kirchner, 2009; Ajami et al., 2011; Heidbüchel et al., 2013; McIntosh et al., 2017). Thus, systems with lower connectivity typically rely on water in the shallow, or dynamic, storage zone. Dynamic storage is part of overall catchment storage and defined as the variation in storage between wet and dry periods (Spence, 2007; Kirchner, 2009; Sayama et al., 2011; Dwivedi et al., 2018). Previous work at Coal Creek suggests that deep storage in the basin is low, and the stream is supplied mostly from water originating in the dynamic storage zone (Zhi et al., 2019; Johnson et al., 2023). During the summer of 2021, we sampled seven springs to capture diverse groundwater chemistry across the catchment, yet median sampled spring chemistry showed ^{222}Rn concentrations three times higher than median modeled contributing groundwater concentrations. This discrepancy in chemical signature between modeled groundwater chemistry and spring samples indicate that deeper groundwater is not a major

contributor to the stream. Rather, streamflow generation at Coal Creek is dependent on shallow flow paths that propagate through the dynamic storage zone.

We used dynamic storage to understand subsurface connectivity, where periods of high dynamic storage are associated with high subsurface connectivity. Our results indicate that as the dynamic storage zone drains (i.e., high to low dynamic storage) throughout the summer, Coal Creek transitions from a high to low hydrologically connected system, relying more on shallow flow paths for streamflow (Figure 10a). This hypothesis is supported by water isotopic evidence that indicates a shift in the stream water source from snow dominance to a higher share of rain in Coal Creek throughout the summer (Figure 6), reductions in the responsiveness of groundwater discharge to the stream following precipitation events (Figure 4), and correlations between dynamic storage and SOI and GW discharge (Figure 10). Interestingly, despite the overall low storage and low connectivity of Coal Creek, groundwater inputs and isotopic responses along Coal Creek varied spatially and were related to changes in storage (Figure 8, Figure 10). These findings are discussed below in detail.

4.1 Stream water origin signals short residence time flow paths dominate in Coal Creek

Coal Creek water origin shifts from more to less snow dominated throughout the summer, with values of SOI ranging from -0.37 to just above 0 (Figure 6). These values are similar to those observed in other monsoon-impacted and montane sites. For example, in the Xiangjiang River basin, China, SOI values ranged between -0.5 and 0 and progressively increased throughout the summer (Xiao et al., 2022). This suggests that summer precipitation in the Xiangjiang River basin is preferentially partitioned to ET, leaving predominantly winter precipitation to feed streamflow. However, SOI values have also been shown to exhibit more dramatic seasonal shifts, exemplified by Allen et al (2019a) across Swiss catchments. Here SOI values ranged from -1 to 1, indicating that more summer precipitation becomes streamflow in these catchments compared to Coal Creek.

At Coal Creek summer precipitation plays an increasingly important role in streamflow generation during dry periods and later in the summer (Figure 6). The increased reliance on summer precipitation for streamflow reflects a shift towards shallower flow paths driven by a decline in connectivity (Covino, 2017). We found a significant, negative relationship between SOI and dynamic storage, indicating that as dynamic storage drains (i.e., more negative dynamic storage values), SOI increases indicating a shift in stream water source towards a higher proportion of rain (Figure 10b). Shifting stream water source throughout the summer is well documented, with many catchments showing shifts towards deep groundwater (Rademacher et al., 2005; Zelazny et al., 2011), and some showing shifts towards shallower flow paths (Spencer et al., 2021; Bush et al., 2023). In catchments impacted by the North American monsoon, summer precipitation can be important for streamflow generation (Carroll et al., 2020). However, when ET demand is high, summer precipitation is often preferentially partitioned to plant uptake (Julander and Clayton, 2018), leading to winter precipitation dominating summer stream flows (Sprenger et al, 2022; Xiao et al., 2022). For Coal Creek, increasing, but still negative, SOI values later in the summer indicate that although summer precipitation becomes more important throughout the summer, streamflow is still snow-dominated suggesting summer precipitation may be partitioned towards ET and away from stream flow generation.

Interestingly, we also observed stream responses to incoming precipitation during periods of higher dynamic storage as well. In general, higher SOI values and more enriched $\delta^{18}O$ values in stream water followed precipitation events in early summer (Figure 4b, Figure 5). It is well documented that precipitation can infiltrate quickly into the subsurface and, in highly permeable areas, discharge into the stream (McDonnell et al., 1990, Wittenberg et al., 2019). We do not observe this quick stream response to precipitation later in the summer, yet we observe an overall enrichment of stream $\delta^{18}O$ values and SOI. We hypothesize that this quick stream response to precipitation is facilitated by rainfall moving through the bedrock fractures during periods of high connectivity, which become disconnected from the stream during periods of low connectivity and therefore no longer transport precipitation to Coal Creek. Later in the summer, precipitation transport leading to enriched values of $\delta^{18}O$, and more positive SOI values, may originate from shallow flow paths connected to the stream in high storage areas, such as the non-fractured zone. Overall, our results suggest that the low-storage fractures respond quickly to incoming precipitation during periods of high connectivity whereas high-storage areas of the catchment may facilitate consistent transport of both summer precipitation through shallow flow paths and snowmelt-recharged groundwater through deeper flow paths.

Climate predictions suggest that snowmelt will occur earlier (Clow, 2010; Kapnick and Hall, 2012) and that the onset of monsoon rains will occur later (Cook and Seager, 2013) with warming, leading to longer summer dry periods. At Coal Creek, where monsoon rains play an important role in sustaining late summer flows, the shift in summer precipitation onset and timing may lead to lower summer flows. In addition, increased ET (Mastrothedoros et al., 2020; Milly and Dunne, 2020) may partition more precipitation away from streamflow generation leading to further reductions in stream flow. With warming, groundwater is expected to become more important for summer stream flows because of shifts in precipitation and melt timing (Mayer and Naman, 2011; Ficklin et al., 2013; Segura et al., 2019), however in catchments like Coal Creek lacking contributions from deep storage, localized groundwater inputs from high storage features can provide significant amounts of flow to streams in the summer (Käser and Hunkeler, 2014) and buffer declines in moisture throughout the summer (Herron and Wilson, 2001). Therefore, evaluating how local geology responds to changes in connectivity is critical for understanding how Coal Creek streamflow may respond under warming conditions.

4.2 Groundwater contribution from fracture vs non-fracture zones show distinct temporal variability

We evaluated the spatial variability in connectivity along the Coal Creek transect through both groundwater flux estimates and responsiveness to incoming precipitation. Groundwater flux values ranged from 0 to 5 x 10^{-5} m s^{-1}, and generally declined throughout the summer as dynamic storage decreased (Figure 8, Figure 10c). Flux values (0 to 5 x 10^{-5} m s^{-1} or 0 to 1.3 m^3 m^{-1} d^{-1} (linear discharge at model unit width 0.3 m)) fall within the range of estimated groundwater fluxes from other applications of this model. This paper is the first application of StreamTran in a montane region, but linear discharge estimations from the Fitzroy River, Australia varied between 0 and 0.5 m^3m^{-1} d^{-1} (Gardner et al., 2011), and in the Daly River, Australia linear discharge varied between 0 and nearly 200 m^3 m^{-1} d^{-1}(Smerdon et al., 2012). Higher groundwater discharge has been observed along reaches near springs, where deeper, regional groundwater discharges to streams (Smerdon et al., 2012; Beisner et al., 2018). In contrast, reaches with lower discharge but more consistent groundwater contribution may reflect the presence of faults and

665 onlapped geology giving rise to permeable preferential flow paths (Gardner et al., 2011),
666 functioning similar to the fractures in Coal Creek.

667 In Coal Creek, groundwater contributed between 60% and 93% of increased flow between
668 the start and end of the modeled reach. The fracture zone contributed between 36% and 77% and
669 the non-fractured zone contributed between 23% and 64% of groundwater influx (Figure 9).
670 Groundwater flux through the fracture zone was highest during early summer when the
671 subsurface is saturated from snowmelt and most hydrologically connected (Figure 8). As
672 connectivity declined throughout the summer, groundwater fluxes through the fractures and the
673 proportion of fracture zone contributions also declined. Studies that have evaluated how fracture
674 flow changes with moisture conditions have found shallow fractured bedrock is highly sensitive
675 to changes in seasonal moisture (Salve et al., 2012) and that fracture flow is significantly slower
676 during periods of lower moisture (Flerchinger et al., 1993). In contrast, groundwater flux through
677 the non-fractured zone is constant throughout the summer, regardless of subsurface connectivity.
678 We used a ratio of fracture zone groundwater flux to non-fractured groundwater flux to evaluate
679 how groundwater contribution from different features changed as connectivity declined and
680 found a strong, significant, positive relationship between fracture: non-fractured groundwater
681 flow and dynamic storage (Figure 10d). The fracture: non-fractured groundwater ratio ranged
682 from > 3 to < 1 and declined as dynamic storage declined indicating that during periods of high
683 connectivity the fracture zone was contributing over three times as much water as the non-
684 fractured zone. In contrast during periods of low connectivity, the non-fractured zone contributed
685 more than double what the fracture zone contributed indicating that this zone becomes a more
686 important source of streamflow when dynamic storage is low. This indicates that groundwater in
687 the non-fractured zone may be originating from an area with high subsurface storage that is
688 hydraulically connected to the stream during periods of low connectivity (Figure 11).
689 Further evaluation of the local geology in the non-fractured zone revealed an alluvial fan at
690 the base of Elk Creek, a perennial tributary to Coal Creek, which may facilitate the transport of
691 water through the subsurface into the stream. Two known hydrologic factors could control
692 subsurface flow through the alluvial fan: 1) water from Elk creek is recharging the alluvial fan
693 and then discharges into this zone, and 2) the alluvial fan is storing and discharging water from a
694 different source than Elk Creek. If water were directly being recharged from Elk Creek through
695 subsurface flow paths, we would expect that the sampling sites in the non-fractured zone would
696 have an isotopic signature that reflects mixing of upstream waters with Elk Creek over time,
697 proportional to the contribution of water from the fractured vs non-fractured zone (Figure 9b).
698 StreamTran model output indicates that groundwater contribution from the fan becomes
699 increasingly important throughout the summer; if water from the fan was originating from Elk
700 Creek, we would expect that the water at the Upstream Elk location would appear chemically
701 similar to Elk Creek, especially later in the summer. Elk Creek remains depleted throughout the
702 summer ($\delta^{18}O$ mean = -16.7, $\delta^{18}O$ SD = 0.5) whereas Upstream Elk becomes more enriched
703 throughout the summer (Figure 4b). Additionally, Coal-15, the site downstream of Elk Creek, is
704 consistently more depleted than the Upstream Elk site (Figure 4b), indicating that the water
705 coming into Coal Creek from Elk Creek is more depleted than that of the water entering through
706 the alluvial fan. We therefore conclude that the alluvial fan is storing water chemically different
707 than Elk Creek.
708 Water flowing through the alluvial fan shows similar isotopic composition to fracture zone
709 water during early summer (i.e., June and July) but begins to deviate starting in August, showing
710 a more depleted signature than fracture zone samples. This suggests that alluvial fan groundwater

may be originating from deeper flow paths, transmitting isotopically depleted snowmelt into the stream later in the summer due to high storage and hydrologic connectivity associated with the fan (Figure 11). The high connectivity of the fan would allow for transport of groundwater into the stream throughout the summer, consistent with the patterns observed in model output. This behavior is also consistent with other studies quantifying the groundwater contribution of alluvial fans to streams; fans have been shown to contribute significant amounts of water to streams (Liu et al., 2004; Gordon et al., 2015), especially during low flow periods (Käser and Hunkeler, 2014).

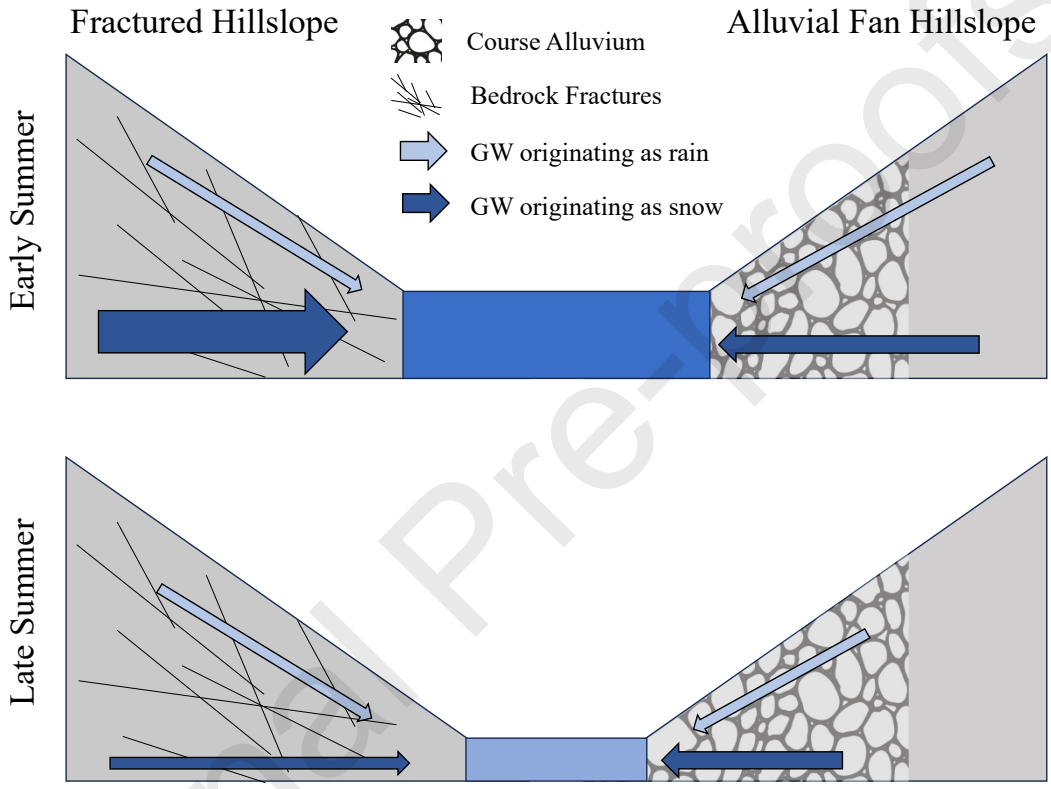

Figure 11: Conceptual diagram developed based on SOI that depicts groundwater originating from snow and rain recharging stream water under fractured and alluvial fan hillslopes during early and late summer. In early summer, groundwater that originated from snow ($\delta_{winterP}$) dominated the fractured hillslope, while in late summer groundwater flow declined and was equally composed of snow and rain. Unlike the fractured hillslope, groundwater that originated from the alluvial fan was consistent in volume and its snow-dominated composition. Early in the summer, the alluvial fan and area upslope of the fan contributed groundwater to the stream, while later in the summer the upslope became disconnected and the alluvial fan was the dominant water source. Overall, stream water composition moved from greater snow ($\delta_{winterP}$) origin in early summer to greater rain origin ($\delta_{summerP}$) in late summer. Height of the arrows indicate the relative proportion of groundwater that originated from rain or snow to the stream.

4.3 Modeling Limitations and Future Work

Our work points towards a need to understand localized groundwater contributions in montane environments, especially those that rely on monsoonal precipitation for summer stream flow generation. While the methods presented in this paper allow for both data driven and

734 modeling analysis of GW-SW interactions, there are several important limitations to consider.
735 The largest sources of error in our model are groundwater ^{222}Rn concentration and gas exchange
736 velocity. Throughout the summer, we measured chemistry from seven springs to capture diverse
737 groundwater behavior, yet when used in the model to predict stream flow and chemistry,
738 modeled stream chemistry drastically diverged from measured stream chemistry. Thus, we
739 concluded that groundwater feeding the springs was not the same groundwater directly
740 contributing to Coal Creek. Gas exchange velocity can be measured using tracer injection tests
741 (Wanninkhof et al., 1990; Maurice et al., 2017), however no tracer test was performed for this
742 work. We used Monte Carlo (MC) simulations to estimate both the groundwater ^{222}Rn
743 concentration and gas exchange velocity. MC bounds for gas exchange velocity were set based
744 on gas exchange literature values for streams of similar size and slope as Coal Creek (Raymond
745 et al., 2012; Ulseth et al., 2019). As expected, gas exchange values varied with discharge, with
746 higher gas exchange values estimated during higher flow periods and lower gas exchange values
747 measured during lower flow. Bounds were set for groundwater ^{222}Rn concentration based on the
748 minimum and maximum ^{222}Rn concentration measured in springs in the watershed. From the MC
749 simulations, groundwater ^{222}Rn concentrations were generally estimated to be low relative to
750 measured ^{222}Rn concentrations, suggesting that groundwater contributing to Coal Creek was
751 relatively young (< 1 week).

752 Gas exchange velocity and groundwater ^{222}Rn concentration parameters exert opposite
753 effects on stream water concentrations: higher gas exchange velocities reduce instream ^{222}Rn
754 concentrations whereas higher groundwater ^{222}Rn concentrations increase instream ^{222}Rn
755 concentrations. We evaluated the relationship between estimated gas exchange velocities and
756 groundwater ^{222}Rn concentrations and found they were negatively correlated and, as expected,
757 gas exchange velocity was positively related to discharge (Figure S4). The median of gas
758 exchange and groundwater ^{222}Rn concentration values across the top 5% best model runs were
759 used to calibrate StreamTran. Pairings of the minimum groundwater ^{222}Rn concentration and
760 minimum gas exchange velocity, and the maximum groundwater ^{222}Rn concentration and
761 maximum gas exchange velocity from the top 5% best models were used to characterize
762 uncertainty around the MC estimated groundwater flux (Table S6). While there was variability in
763 estimated GW flux across the range of values retained in the top 5% of AIC values (Figure 12),
764 declining trends in groundwater flux throughout the summer and variability across the reach
765 exceeded uncertainty. Visual inspection of model output using MC estimated values showed a
766 good fit between measured and modeled stream discharge (Figure 7), however, near stream
767 piezometers and tracer injection tests likely would have provided better constraints on values for
768 groundwater ^{222}Rn concentrations and gas exchange velocity.

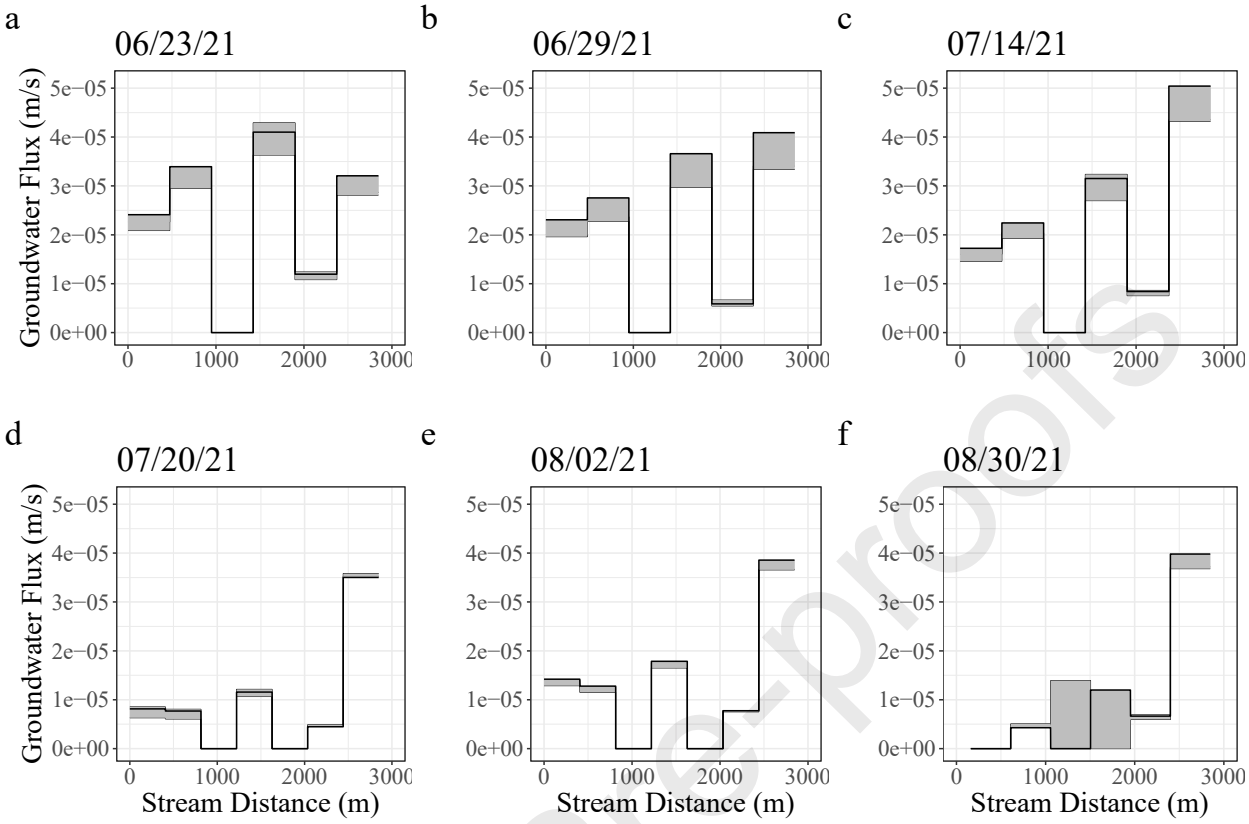

Figure 12: Modeled groundwater fluxes (black line) and uncertainty (grey shading) estimated using the minimum paired groundwater ^{222}Rn and gas exchange velocity, and maximum paired groundwater ^{222}Rn and gas exchange velocity from the top 5% of AIC values from the Monte Carlo analysis for each modeled event.

In StreamTran, estimations of groundwater flux and stream water ^{222}Rn concentrations are sensitive to the distance between sampling locations. Groundwater ^{222}Rn degasses upon contact with the atmosphere, and in small streams with high gas exchange velocity, changes in ^{222}Rn can happen rapidly. The scale length describes how far apart samples should be taken given discharge and stream geometry (Cook et al., 2006). Scale lengths in Coal Creek vary between 28 and 101 meters depending on stream reach location and discharge but are shorter than the distances between samples we used (161 – 787 meters). We acknowledge that this sample design may lead to an underestimation of groundwater inputs, especially in the portion of the reach further upstream from sampling locations. However, the goal of using this model was to compare how spatial groundwater discharge varied across time. While the reach length is longer than the length scale, the sampling locations were held constant across the sampling events and therefore we are still able to look at differences with time and interpret changes between events.

In addition to limitations imposed by data availability, StreamTran has several assumptions that influence the predicted volume of groundwater discharge. StreamTran does not consider hyporheic exchange, which can contribute substantial amounts of ^{222}Rn to streams (Cook et al., 2006; Bourke et al., 2014; Cartwright and Hoffman, 2016). Hyporheic exchange describes the exchange of stream water through alluvial aquifers through flow paths that begin and end in the stream channel (Gooseff, 2010). While we acknowledge that the omission of hyporheic exchange in our model may lead to overestimations of groundwater flux, along reaches longer than

hyporheic flow paths (i.e., cm to tens of meters) (Boano et al., 2014), hyporheic exchange does not increase total stream flow. Along our modeled reach, streamflow increases substantially with limited input from tributaries, indicating groundwater contributions must be driving flow increases. StreamTran accounts for the gaining nature of the reach by fitting not only ^{222}Rn concentrations but also measured discharge. Therefore, the model fit is weighted toward groundwater discharge that increases stream flow, and we can be confident that increasing streamflow and peaks in ^{222}Rn concentration indicate groundwater contribution and not Rn input from hyporheic exchange. Additionally, the groundwater fluxes estimated by the model are used for comparison over time; evaluating relative differences among synoptic events is valid even if estimations are high.

StreamTran assumes steady state conditions of spatially and temporally input parameters, including stream temperature, evaporation, gas exchange velocity, groundwater ^{222}Rn concentration, and stream slope. It is well documented that groundwater ^{222}Rn concentration can be spatially variable at Coal Creek (Table 2) and in other streams (McClymont et al., 2012; Floriancic et al., 2018). Gas exchange velocity is influenced by factors such as turbulence, depth, slope, and stream temperature that vary across the modeled stream reach. Finally, StreamTran uses a linear interpolation of width, depth, and area and assumes a rectangular stream channel between measurement locations which erases much of the complex channel morphology present in small headwater streams (Schneider et al., 2015). When we included temporal variation of all input parameters between sampling dates using the Monte Carlo approach, we observed that patterns in modeled groundwater discharge in time and space outweigh the uncertainty introduced by steady state behavior (Figure 12). With similar datasets, this could be applied to other river systems (Beisner et al., 2018) to understand localized and regional groundwater contribution to streamflow.

Future work at Coal Creek could leverage this new model of groundwater flow to understand solute transport. The Coal Creek watershed, and many other watersheds in the Rocky Mountains, are heavily mined and mineralized leading to concerns about metal transport into streams. Coal Creek serves as the drinking water supply for the town of Crested Butte, and previous work has identified high concentrations of zinc, cadmium, and copper in stream water (Manning et al., 2007; Verplanck et al., 2009). A better understanding of fracture and alluvial fan groundwater contributions may help elucidate source and timing of metal fluxes into Coal Creek.

5.0 Conclusion

Understanding local controls on GW-SW interactions is critical as groundwater becomes more important for summer streamflow generation under warmer conditions. We used spatial and temporal ^{222}Rn and water isotope sampling along a three km reach of a Colorado River headwater stream to assess how bedrock fractures control GW-SW interactions throughout the summer. The model application presented here is transferable to other stream reaches with similar geochemistry data to understand how streamflow generation processes shift through time and space. We characterized changes in subsurface hydrologic connectivity throughout the summer using dynamic storage, and found the catchment shifts from high to low hydrologic connectivity over the summer. We observed variable responses to declining connectivity between geologic features. During early summer, groundwater contributions through the fracture zone dominated groundwater flux along the reach but declined as summer progressed. In

contrast, groundwater contributions from the non-fractured zone were constant throughout the study and dominated in late summer when fracture contributions were low. We hypothesize that groundwater in the non-fractured zone is dominantly sourced from a high-storage alluvial fan at the base of Elk Creek that is connected to Coal Creek throughout the summer and provides consistent groundwater influx. Throughout the summer, streamflow origin shifted from more to less snow dominated reflecting the important role that monsoonal precipitation plays in streamflow generation during the late summer. At the catchment scale, we observed significant relationships between dynamic storage and water isotope values, groundwater discharge, and the ratio of fracture to non-fractured zone groundwater contribution indicating that periods of higher connectivity led to more snow dominated stream water, higher groundwater discharge, and a higher proportion of fracture zone groundwater in Coal Creek. Overall, we observed that at the catchment scale shallow flow paths became more important for streamflow generation during low hydrologic connectivity conditions, but local geologic features responded differently to changes in moisture based on their storage. Under warmer conditions, groundwater and monsoon rains may become more important for sustaining summer flows. Based on this work, we expect high storage features, such as alluvial fans, to become more important for sustaining streamflow under warming. Additionally, we expect a higher proportion of late season streamflow to originate from monsoon rains transported through shallow flow paths as deeper groundwater transported through low storage features may become disconnected from the stream earlier in the summer. To better understand streamflow generation processes in montane catchments, additional assessment of groundwater and stream response to warming and monsoon rain is critical.

Data Availability

Data is available on ESS-DIVE: doi:10.15485/2283437

Code Availability

Related code is available in Zenodo repository: https://doi.org/10.5281/zenodo.10045527

Competing Interests

The contact author has declared that none of the authors has any competing interests.

Acknowledgements

This material is based upon work supported by the National Science Foundation under Grant No. (PL Sullivan: NSF 2034232, and 2012796) and the Department of Energy under Grant No. (PL Sullivan + L Li: DE-SC0020146). K.H.W., J.N.C., R.W.H.C and M.S. are supported by the US Department of Energy Office of Science under contract DE-AC02-05CH11231 as part of Lawrence Berkeley National Laboratory Watershed Function Science Focus Area.

References

Ajami, H., Troch, P. A., Maddock III, T., Meixner, T., & Eastoe, C. (2011). Quantifying mountain block recharge by means of catchment-scale storage-discharge relationships. *Water Resources Research*, *47*(4). https://doi.org/10.1029/2010WR009598

873 Allen, S. T., Kirchner, J. W., Braun, S., Siegwolf, R. T. W., & Goldsmith, G. R. (2019). Seasonal
874 origins of soil water used by trees. *Hydrology and Earth System Sciences*, *23*(2), 1199–
875 1210. https://doi.org/10.5194/hess-23-1199-2019

876 Allen, S. T., von Freyberg, J., Weiler, M., Goldsmith, G. R., & Kirchner, J. W. (2019). The
877 Seasonal Origins of Streamwater in Switzerland. *Geophysical Research Letters*, *46*(17–
878 18), 10425–10434. https://doi.org/10.1029/2019GL084552

879 Andermann, C., Longuevergne, L., Bonnet, S., Crave, A., Davy, P., & Gloaguen, R. (2012).
880 Impact of transient groundwater storage on the discharge of Himalayan rivers. *Nature*
881 *Geoscience*, *5*(2), 127–132. https://doi.org/10.1038/ngeo1356

882 Avery, E., Bibby, R., Visser, A., Esser, B., & Moran, J. (2018). Quantification of Groundwater
883 Discharge in a Subalpine Stream Using Radon-222. *Water*, *10*(2), Article 2.
884 https://doi.org/10.3390/w10020100

885 Azmat, M., Liaqat, U. W., Qamar, M. U., & Awan, U. K. (2017). Impacts of changing climate
886 and snow cover on the flow regime of Jhelum River, Western Himalayas. *Regional*
887 *Environmental Change; Dordrecht*, *17*(3), 813–825.
888 http://dx.doi.org.ezproxy.proxy.library.oregonstate.edu/10.1007/s10113-016-1072-6

889 Banks, E. W., Simmons, C. T., Love, A. J., Cranswick, R., Werner, A. D., Bestland, E. A.,
890 Wood, M., & Wilson, T. (2009). Fractured bedrock and saprolite hydrogeologic controls
891 on groundwater/surface-water interaction: A conceptual model (Australia). *Hydrogeology*
892 *Journal*, *17*(8), 1969–1989. https://doi.org/10.1007/s10040-009-0490-7

893 Banks, E. W., Simmons, C. T., Love, A. J., & Shand, P. (2011). Assessing spatial and temporal
894 connectivity between surface water and groundwater in a regional catchment: Implications
895 for regional scale water quantity and quality. *Journal of Hydrology*, *404*(1), 30–49.
896 https://doi.org/10.1016/j.jhydrol.2011.04.017

897 Bavay, M., Lehning, M., Jonas, T., & Löwe, H. (2009). Simulations of future snow cover and
898 discharge in Alpine headwater catchments. *Hydrological Processes*, *23*(1), 95–108.
899 https://doi.org/10.1002/hyp.7195

900 Beisner, K. R., Gardner, W. P., & Hunt, A. G. (2018). Geochemical characterization and
901 modeling of regional groundwater contributing to the Verde River, Arizona between
902 Mormon Pocket and the USGS Clarkdale gage. *Journal of Hydrology*, *564*, 99–114.
903 https://doi.org/10.1016/j.jhydrol.2018.06.078

904 Blume, T., & van Meerveld, H. J. (Ilja). (2015). From hillslope to stream: Methods to investigate
905 subsurface connectivity. *WIREs Water*, *2*(3), 177–198. https://doi.org/10.1002/wat2.1071

906 Boano, F., Harvey, J. W., Marion, A., Packman, A. I., Revelli, R., Ridolfi, L., & Wörman, A.
907 (2014). Hyporheic flow and transport processes: Mechanisms, models, and biogeochemical
908 implications. *Reviews of Geophysics*, *52*(4), 603–679.
909 https://doi.org/10.1002/2012RG000417

910 Bourke, S. A., Cook, P. G., Shanafield, M., Dogramaci, S., & Clark, J. F. (2014).
911 Characterisation of hyporheic exchange in a losing stream using radon-222. *Journal of*
912 *Hydrology*, *519*, 94–105. https://doi.org/10.1016/j.jhydrol.2014.06.057

913 Bozdogan, H. (1987). Model selection and Akaike's Information Criterion (AIC): The general
914 theory and its analytical extensions. *Psychometrika*, *52*(3), 345–370.
915 https://doi.org/10.1007/BF02294361

916 Brooks, P. D., Gelderloos, A., Wolf, M. A., Jamison, L. R., Strong, C., Solomon, D. K., Bowen,
917 G. J., Burian, S., Tai, X., Arens, S., Briefer, L., Kirkham, T., & Stewart, J. (2021).
918 Groundwater-Mediated Memory of Past Climate Controls Water Yield in Snowmelt-
919 Dominated Catchments. *Water Resources Research*, *57*(10), e2021WR030605.
920 https://doi.org/10.1029/2021WR030605

921 Bush, S. A., Birch, A. L., Warix, S. R., Sullivan, P. L., Gooseff, M. N., McKnight, D. M., &
922 Barnard, H. R. (2023). Dominant source areas shift seasonally from longitudinal to lateral
923 contributions in a montane headwater stream. *Journal of Hydrology*, *617*, 129134.
924 https://doi.org/10.1016/j.jhydrol.2023.129134

925 Carroll, R. W. H., Bearup, L. A., Brown, W., Dong, W., Bill, M., & Willlams, K. H. (2018).
926 Factors controlling seasonal groundwater and solute flux from snow-dominated basins.
927 *Hydrological Processes*, *32*(14), 2187–2202. https://doi.org/10.1002/hyp.13151

928 Carroll, R. W. H., Gochis, D., & Williams, K. H. (2020). Efficiency of the Summer Monsoon in
929 Generating Streamflow Within a Snow-Dominated Headwater Basin of the Colorado
930 River. *Geophysical Research Letters*, *47*(23), e2020GL090856.
931 https://doi.org/10.1029/2020GL090856

932 Cartwright, I., & Hofmann, H. (2016). Using radon to understand parafluvial flows and the
933 changing locations of groundwater inflows in the Avon River, southeast Australia.
934 *Hydrology and Earth System Sciences*, *20*(9), 3581–3600. https://doi.org/10.5194/hess-20-
935 3581-2016

936 Cook, B. I., & Seager, R. (2013). The response of the North American Monsoon to increased
937 greenhouse gas forcing. *Journal of Geophysical Research: Atmospheres*, *118*(4), 1690–
938 1699. https://doi.org/10.1002/jgrd.50111

939 Cook, P. G., & Herczeg, A. L. (2000). *Environmental tracers in subsurface hydrology*. Springer
940 Science + Business Media, LLC.

941 Cook, P. G., Lamontagne, S., Berhane, D., & Clark, J. F. (2006). Quantifying groundwater
942 discharge to Cockburn River, southeastern Australia, using dissolved gas tracers 222Rn and
943 SF6. *Water Resources Research*, *42*(10). https://doi.org/10.1029/2006WR004921

944 Covino, T. (2017). Hydrologic connectivity as a framework for understanding biogeochemical
945 flux through watersheds and along fluvial networks. *Geomorphology*, *277*, 133–144.
946 https://doi.org/10.1016/j.geomorph.2016.09.030

947 Cowie, R. M., Knowles, J. F., Dailey, K. R., Williams, M. W., Mills, T. J., & Molotch, N. P.
948 (2017). Sources of streamflow along a headwater catchment elevational gradient. *Journal*
949 *of Hydrology*, *549*, 163–178. https://doi.org/10.1016/j.jhydrol.2017.03.044

950 Dwivedi, R., Meixner, T., McIntosh, J. C., Ferré, P. A. T., Eastoe, C. J., Niu, G.-Y., Minor, R.
951 L., Barron-Gafford, G. A., & Chorover, J. (2019). Hydrologic functioning of the deep
952 critical zone and contributions to streamflow in a high-elevation catchment: Testing of
953 multiple conceptual models. *Hydrological Processes*, *33*(4), 476–494.
954 https://doi.org/10.1002/hyp.13363

955 Ehsani, M. R., & Behrangi, A. (2022). A comparison of correction factors for the systematic
956 gauge-measurement errors to improve the global land precipitation estimate. *Journal of*
957 *Hydrology*, *610*, 127884. https://doi.org/10.1016/j.jhydrol.2022.127884

958 Ficklin, D. L., Stewart, I. T., & Maurer, E. P. (2013). Climate Change Impacts on Streamflow
959 and Subbasin-Scale Hydrology in the Upper Colorado River Basin. *PLOS ONE*, *8*(8),
960 e71297. https://doi.org/10.1371/journal.pone.0071297

961 Fischer, B. M. C., Rinderer, M., Schneider, P., Ewen, T., & Seibert, J. (2015). Contributing
962 sources to baseflow in pre-alpine headwaters using spatial snapshot sampling.
963 *Hydrological Processes*, *29*(26), 5321–5336. https://doi.org/10.1002/hyp.10529

964 Flerchinger, G., Deng, Y., & Cooley, K. (1993). *Groundwater response to snowmelt in a*
965 *mountainous watershed: Testing of a conceptual model*. https://doi.org/10.1016/0022-
966 1694(93)90146-Z

967 Floriancic, M. G., van Meerveld, I., Smoorenburg, M., Margreth, M., Naef, F., Kirchner, J. W.,
968 & Molnar, P. (2018). Spatio-temporal variability in contributions to low flows in the high
969 Alpine Poschiavino catchment. *Hydrological Processes*, *32*(26), 3938–3953.
970 https://doi.org/10.1002/hyp.13302

971 Gardner, W. P., Harrington, G. A., Solomon, D. K., & Cook, P. G. (2011). Using terrigenic 4He
972 to identify and quantify regional groundwater discharge to streams. *Water Resources*
973 *Research*, *47*(6). https://doi.org/10.1029/2010WR010276

974 Gaskill, D. L. (1991). *Geologic map of the Gothic Quadrangle, Gunnison County, Colorado*.

975 Genereux, D. P., Hemond, H. F., & Mulholland, P. J. (1993). Use of radon-222 and calcium as
976 tracers in a three-end-member mixing model for streamflow generation on the West Fork
977 of Walker Branch Watershed. *Journal of Hydrology*, *142*(1), 167–211.
978 https://doi.org/10.1016/0022-1694(93)90010-7

979 Gleeson, T., Manning, A. H., Popp, A., Zane, M., & Clark, J. F. (2018). The suitability of using
980 dissolved gases to determine groundwater discharge to high gradient streams. *Journal of*
981 *Hydrology*, *557*, 561–572. https://doi.org/10.1016/j.jhydrol.2017.12.022

Gooseff, M. N. (2010). Defining Hyporheic Zones – Advancing Our Conceptual and Operational Definitions of Where Stream Water and Groundwater Meet. *Geography Compass*, *4*(8), 945–955. https://doi.org/10.1111/j.1749-8198.2010.00364.x

Gordon, R. P., Lautz, L. K., McKenzie, J. M., Mark, B. G., Chavez, D., & Baraer, M. (2015). Sources and pathways of stream generation in tropical proglacial valleys of the Cordillera Blanca, Peru. *Journal of Hydrology*, *522*, 628–644. https://doi.org/10.1016/j.jhydrol.2015.01.013

Guyer, J. E., Wheeler, D., & Warren, J. A. (2009). FiPy: Partial Differential Equations with Python. *Computing in Science & Engineering*, *11*(3), 6–15. https://doi.org/10.1109/MCSE.2009.52

Heidbüchel, I., Troch, P. A., & Lyon, S. W. (2013). Separating physical and meteorological controls of variable transit times in zero-order catchments. *Water Resources Research*, *49*(11), 7644–7657. https://doi.org/10.1002/2012WR013149

Herron, N., & Wilson, C. (2001). A water balance approach to assessing the hydrologic buffering potential of an alluvial fan. *Water Resources Research*, *37*(2), 341–351. https://doi.org/10.1029/2000WR900253

Hua, D., Hao, X., Zhang, Y., & Qin, J. (2020). Uncertainty assessment of potential evapotranspiration in arid areas, as estimated by the Penman-Monteith method. *Journal of Arid Land*, *12*(1), 166–180. https://doi.org/10.1007/s40333-020-0093-7

Hubbard, S. S., Williams, K. H., Agarwal, D., Banfield, J., Beller, H., Bouskill, N., Brodie, E., Carroll, R., Dafflon, B., Dwivedi, D., Falco, N., Faybishenko, B., Maxwell, R., Nico, P., Steefel, C., Steltzer, H., Tokunaga, T., Tran, P. A., Wainwright, H., & Varadharajan, C. (2018). The East River, Colorado, Watershed: A Mountainous Community Testbed for Improving Predictive Understanding of Multiscale Hydrological–Biogeochemical Dynamics. *Vadose Zone Journal*, *17*(1), 180061. https://doi.org/10.2136/vzj2018.03.0061

Jencso, K. G., McGlynn, B. L., Gooseff, M. N., Bencala, K. E., & Wondzell, S. M. (2010). Hillslope hydrologic connectivity controls riparian groundwater turnover: Implications of catchment structure for riparian buffering and stream water sources. *Water Resources Research*, *46*(10). https://doi.org/10.1029/2009WR008818

Johnson, K. (2023). hydrokeira/CoalCreekGW_JoH: Groundwater Flux Code: Coal Creek (v1.0.1). Zenodo. https://doi.org/10.5281/zenodo.10045527

Johnson, K., Harpold, A., Carroll, R. W. H., Barnard, H., Raleigh, M. S., Segura, C., Li, L., Williams, K. H., Dong, W., & Sullivan, P. L. (2023). Leveraging Groundwater Dynamics to Improve Predictions of Summer Low-Flow Discharges. *Water Resources Research*, *59*(8), e2023WR035126. https://doi.org/10.1029/2023WR035126

Julander, R. P., & Clayton, J. A. (2018). Determining the proportion of streamflow that is generated by cold season processes versus summer rainfall in Utah, USA. *Journal of Hydrology: Regional Studies*, *17*, 36–46. https://doi.org/10.1016/j.ejrh.2018.04.005

1020 Kapnick, S., & Hall, A. (2012). Causes of recent changes in western North American snowpack.
1021 *Climate Dynamics*, *38*(9–10), 1885–1900. https://doi.org/10.1007/s00382-011-1089-y

1022 Käser, D., & Hunkeler, D. (2016). Contribution of alluvial groundwater to the outflow of
1023 mountainous catchments. *Water Resources Research*, *52*(2), 680–697.
1024 https://doi.org/10.1002/2014WR016730

1025 Kingston, D. G., Todd, M. C., Taylor, R. G., Thompson, J. R., & Arnell, N. W. (2009).
1026 Uncertainty in the estimation of potential evapotranspiration under climate change.
1027 *Geophysical Research Letters*, *36*(20). https://doi.org/10.1029/2009GL040267

1028 Kirchner, J. W. (2009). Catchments as simple dynamical systems: Catchment characterization,
1029 rainfall-runoff modeling, and doing hydrology backward. *Water Resources Research*,
1030 *45*(2). https://doi.org/10.1029/2008WR006912

1031 Larson, L. W., & Peck, E. L. (1974). Accuracy of precipitation measurements for hydrologic
1032 modeling. *Water Resources Research*, *10*(4), 857–863.
1033 https://doi.org/10.1029/WR010i004p00857

1034 Liao, F., Cardenas, M. B., Ferencz, S. B., Chen, X., & Wang, G. (2021). Tracing Bank Storage
1035 and Hyporheic Exchange Dynamics Using 222Rn: Virtual and Field Tests and Comparison
1036 With Other Tracers. *Water Resources Research*, *57*(5), e2020WR028960.
1037 https://doi.org/10.1029/2020WR028960

1038 Liu, F., Williams, M. W., & Caine, N. (2004). Source waters and flow paths in an alpine
1039 catchment, Colorado Front Range, United States. *Water Resources Research*, *40*(9).
1040 https://doi.org/10.1029/2004WR003076

1041 Ludwig, KR. User's manual for Isoplot version 3.75–4.15: A geochronological toolkit for
1042 Microsoft Excel: Berkeley Geochronological Center Special Publication 5

1043 Manning, A.H., Verplanck, P.L., Mast, M.A., and Wanty, R.B., 2008, Hydrogeochemical
1044 investigation of the Standard Mine vicinity, upper Elk Creek Basin, Colorado: U.S.
1045 Geological Survey Scientific Investigations Report 2007–5265, 131 p.

1046 Mastrotheodoros, T., Pappas, C., Molnar, P., Burlando, P., Manoli, G., Parajka, J., Rigon, R.,
1047 Szeles, B., Bottazzi, M., Hadjidoukas, P., & Fatichi, S. (2020). More green and less blue
1048 water in the Alps during warmer summers. *Nature Climate Change*, *10*(2), Article 2.
1049 https://doi.org/10.1038/s41558-019-0676-5

1050 Maurice, L., Rawlins, B. G., Farr, G., Bell, R., & Gooddy, D. C. (2017). The Influence of Flow
1051 and Bed Slope on Gas Transfer in Steep Streams and Their Implications for Evasion of
1052 CO2. *Journal of Geophysical Research: Biogeosciences*, *122*(11), 2862–2875.
1053 https://doi.org/10.1002/2017JG004045

1054 Mayer, T. D., & Naman, S. W. (2011). Streamflow Response to Climate as Influenced by
1055 Geology and Elevation1. *JAWRA Journal of the American Water Resources Association*,
1056 *47*(4), 724–738. https://doi.org/10.1111/j.1752-1688.2011.00537.x

McClymont, A. F., Hayashi, M., Bentley, L. R., & Liard, J. (2012). Locating and characterising groundwater storage areas within an alpine watershed using time-lapse gravity, GPR and seismic refraction methods. *Hydrological Processes*, *26*(12), 1792–1804. https://doi.org/10.1002/hyp.9316

McDonnell, J. J. (1990). A Rationale for Old Water Discharge Through Macropores in a Steep, Humid Catchment. *Water Resources Research*, *26*(11), 2821–2832. https://doi.org/10.1029/WR026i011p02821

McIntosh, J. C., Schaumberg, C., Perdrial, J., Harpold, A., Vázquez-Ortega, A., Rasmussen, C., Vinson, D., Zapata-Rios, X., Brooks, P. D., Meixner, T., Pelletier, J., Derry, L., & Chorover, J. (2017). Geochemical evolution of the Critical Zone across variable time scales informs concentration-discharge relationships: Jemez River Basin Critical Zone Observatory. *Water Resources Research*, *53*(5), 4169–4196. https://doi.org/10.1002/2016WR019712

Milly, P. C. D., & Dunne, K. A. (2020). Colorado River flow dwindles as warming-driven loss of reflective snow energizes evaporation. *Science (New York, N.Y.)*, *367*(6483), 1252–1255. https://doi.org/10.1126/science.aay9187

Mote, P. W., Li, S., Lettenmaier, D. P., Xiao, M., & Engel, R. (2018). Dramatic declines in snowpack in the western US. *Npj Climate and Atmospheric Science*, *1*(1), 2. https://doi.org/10.1038/s41612-018-0012-1

Mullinger, N. J., Pates, J. M., Binley, A. M., & Crook, N. P. (2009). Controls on the spatial and temporal variability of 222Rn in riparian groundwater in a lowland Chalk catchment. *Journal of Hydrology*, *376*(1), 58–69. https://doi.org/10.1016/j.jhydrol.2009.07.015

Oxtobee, J. P. A., & Novakowski, K. S. (2003). Ground Water/Surface Water Interaction in a Fractured Rock Aquifer. *Groundwater*, *41*(5), 667–681. https://doi.org/10.1111/j.1745-6584.2003.tb02405.x

Peterson, R. N., Santos, I. R., & Burnett, W. C. (2010). Evaluating groundwater discharge to tidal rivers based on a Rn-222 time-series approach. *Estuarine, Coastal and Shelf Science*, *86*(2), 165–178. https://doi.org/10.1016/j.ecss.2009.10.022

Rademacher, L. K., Clark, J. F., Clow, D. W., & Hudson, G. B. (2005). Old groundwater influence on stream hydrochemistry and catchment response times in a small Sierra Nevada catchment: Sagehen Creek, California. *Water Resources Research*, *41*(2). https://doi.org/10.1029/2003WR002805

Raymond, P. A., Zappa, C. J., Butman, D., Bott, T. L., Potter, J., Mulholland, P., Laursen, A. E., McDowell, W. H., & Newbold, D. (2012). Scaling the gas transfer velocity and hydraulic geometry in streams and small rivers. *Limnology and Oceanography: Fluids and Environments*, *2*(1), 41–53. https://doi.org/10.1215/21573689-1597669

1093 Ryken, A. C., Gochis, D., & Maxwell, R. M. (2022). Unravelling groundwater contributions to
1094 evapotranspiration and constraining water fluxes in a high-elevation catchment.
1095 *Hydrological Processes*, *36*(1), e14449. https://doi.org/10.1002/hyp.14449

1096 Safeeq, M., Grant, G. E., Lewis, S. L., & Tague, Christina. L. (2013). Coupling snowpack and
1097 groundwater dynamics to interpret historical streamflow trends in the western United States:
1098 COUPLING SNOWPACK AND GROUNDWATER DYNAMICS TO INTERPRET
1099 STREAMFLOW. *Hydrological Processes*, *27*(5), 655–668.
1100 https://doi.org/10.1002/hyp.9628

1101 Salve, R., Rempe, D. M., & Dietrich, W. E. (2012). Rain, rock moisture dynamics, and the rapid
1102 response of perched groundwater in weathered, fractured argillite underlying a steep
1103 hillslope. *Water Resources Research*, *48*(11). https://doi.org/10.1029/2012WR012583

1104 Sayama, T., McDonnell, J. J., Dhakal, A., & Sullivan, K. (2011). How much water can a
1105 watershed store? *Hydrological Processes*, *25*(25), 3899–3908.
1106 https://doi.org/10.1002/hyp.8288

1107 Schmidt, A., Gibson, J. J., Santos, I. R., Schubert, M., Tattrie, K., & Weiss, H. (2010). The
1108 contribution of groundwater discharge to the overall water budget of two typical Boreal
1109 lakes in Alberta/Canada estimated from a radon mass balance. *Hydrology and Earth*
1110 *System Sciences*, *14*(1), 79–89. https://doi.org/10.5194/hess-14-79-2010

1111 Schneider, J. M., Rickenmann, D., Turowski, J. M., & Kirchner, J. W. (2015). Self-adjustment of
1112 stream bed roughness and flow velocity in a steep mountain channel. *Water Resources*
1113 *Research*, *51*(10), 7838–7859. https://doi.org/10.1002/2015WR016934

1114 Schubert, M., Siebert, C., Knoeller, K., Roediger, T., Schmidt, A., & Gilfedder, B. (2020).
1115 Investigating Groundwater Discharge into a Major River under Low Flow Conditions
1116 Based on a Radon Mass Balance Supported by Tritium Data. *Water*, *12*(10), 2838.
1117 https://doi.org/10.3390/w12102838

1118 Segura, C., Noone, D., Warren, D., Jones, J. A., Tenny, J., & Ganio, L. M. (2019). Climate,
1119 Landforms, and Geology Affect Baseflow Sources in a Mountain Catchment. *Water*
1120 *Resources Research*, *55*(7), 5238–5254. https://doi.org/10.1029/2018WR023551

1121 Singh, N. K., Emanuel, R. E., & McGlynn, B. L. (2016). Variability in isotopic composition of
1122 base flow in two headwater streams of the southern Appalachians. *Water Resources*
1123 *Research*, *52*(6), 4264–4279. https://doi.org/10.1002/2015WR018463

1124 Smerdon, B. D., & Gardner, W. P. (2022). Characterizing groundwater flow paths in an
1125 undeveloped region through synoptic river sampling for environmental tracers.
1126 *Hydrological Processes*, *36*(1), e14464. https://doi.org/10.1002/hyp.14464

1127 Smerdon, B. D., Payton Gardner, W., Harrington, G. A., & Tickell, S. J. (2012). Identifying the
1128 contribution of regional groundwater to the baseflow of a tropical river (Daly River,
1129 Australia). *Journal of Hydrology*, *464–465*, 107–115.
1130 https://doi.org/10.1016/j.jhydrol.2012.06.058

1131 Somers, L. D., & McKenzie, J. M. (2020a). A review of groundwater in high mountain
1132 environments. *WIREs Water*, *7*(6), e1475. https://doi.org/10.1002/wat2.1475

1133 Somers, L. D., & McKenzie, J. M. (2020b). A review of groundwater in high mountain
1134 environments. *WIREs Water*, *7*(6), e1475. https://doi.org/10.1002/wat2.1475

1135 Somers, L. D., McKenzie, J. M., Mark, B. G., Lagos, P., Ng, G.-H. C., Wickert, A. D., Yarleque,
1136 C., Baraër, M., & Silva, Y. (2019). Groundwater Buffers Decreasing Glacier Melt in an
1137 Andean Watershed—But Not Forever. *Geophysical Research Letters*, *46*(22), 13016–
1138 13026. https://doi.org/10.1029/2019GL084730

1139 Spence, C. (2007). On the relation between dynamic storage and runoff: A discussion on
1140 thresholds, efficiency, and function. *Water Resources Research*, *43*(12).
1141 https://doi.org/10.1029/2006WR005645

1142 Spencer, S. A., Anderson, A. E., Silins, U., & Collins, A. L. (2021). Hillslope and groundwater
1143 contributions to streamflow in a Rocky Mountain watershed underlain by glacial till and
1144 fractured sedimentary bedrock. *Hydrology and Earth System Sciences*, *25*(1), 237–255.
1145 https://doi.org/10.5194/hess-25-237-2021

1146 Sprenger, M., Carroll, R. W. H., Dennedy-Frank, J., Siirila-Woodburn, E. R., Newcomer, M. E.,
1147 Brown, W., Newman, A., Beutler, C., Bill, M., Hubbard, S. S., & Williams, K. H. (2022).
1148 Variability of Snow and Rainfall Partitioning Into Evapotranspiration and Summer
1149 Runoff Across Nine Mountainous Catchments. *Geophysical Research Letters*, *49*(13),
1150 e2022GL099324. https://doi.org/10.1029/2022GL099324

1151 Stewart, I. T., Cayan, D. R., & Dettinger, M. D. (2005). Changes toward Earlier Streamflow
1152 Timing across Western North America. *Journal of Climate*, *18*(8), 1136–1155.
1153 https://doi.org/10.1175/JCLI3321.1

1154 Ulseth, A. J., Hall, R. O., Boix Canadell, M., Madinger, H. L., Niayifar, A., & Battin, T. J.
1155 (2019). Distinct air–water gas exchange regimes in low- and high-energy streams. *Nature*
1156 *Geoscience*, *12*(4), Article 4. https://doi.org/10.1038/s41561-019-0324-8

1157 Verplanck, P.L., Manning, A.H., Graves, J.T., McCleskey, R.B., Todorov, Todor, and Lamothe,
1158 P.J., 2010, Geochemistry of Standard Mine waters, Gunnison County, Colorado, July
1159 2009: U.S. Geological Survey Open-File Report 2009–1292, 21 p.

1160 Viviroli, D., Dürr, H. H., Messerli, B., Meybeck, M., & Weingartner, R. (2007). Mountains of
1161 the world, water towers for humanity: Typology, mapping, and global significance.
1162 *Water Resources Research*, *43*(7). https://doi.org/10.1029/2006WR005653

1163 Viviroli, D., Kummu, M., Meybeck, M., Kallio, M., & Wada, Y. (2020). Increasing dependence
1164 of lowland populations on mountain water resources. *Nature Sustainability*, *3*(11), Article
1165 11. https://doi.org/10.1038/s41893-020-0559-9

Wanninkhof, R., Mulholland, P. J., & Elwood, J. W. (1990). Gas exchange rates for a first-order stream determined with deliberate and natural tracers. *Water Resources Research*, *26*(7), 1621–1630. https://doi.org/10.1029/WR026i007p01621

Webb, J. R., Santos, I. R., Robson, B., Macdonald, B., Jeffrey, L., & Maher, D. T. (2017). Constraining the annual groundwater contribution to the water balance of an agricultural floodplain using radon: The importance of floods. *Water Resources Research*, *53*(1), 544–562. https://doi.org/10.1002/2016WR019735

Westerhoff, R. S. (2015). Using uncertainty of Penman and Penman–Monteith methods in combined satellite and ground-based evapotranspiration estimates. *Remote Sensing of Environment*, *169*, 102–112. https://doi.org/10.1016/j.rse.2015.07.021

Wittenberg, H., Aksoy, H., & Miegel, K. (2019). Fast response of groundwater to heavy rainfall. *Journal of Hydrology*, *571*, 837–842. https://doi.org/10.1016/j.jhydrol.2019.02.037

Xiao, X., Zhang, X., Wu, H., Zhang, C., & Han, L. (2022). Stable isotopes of surface water and groundwater in a typical subtropical basin in south-central China: Insights into the young water fraction and its seasonal origin. *Hydrological Processes*, *36*(4), e14574. https://doi.org/10.1002/hyp.14574

Żelazny, M., Astel, A., Wolanin, A., & Małek, S. (2011a). Spatiotemporal dynamics of spring and stream water chemistry in a high-mountain area. *Environmental Pollution*, *159*(5), 1048–1057. https://doi.org/10.1016/j.envpol.2010.11.021

Żelazny, M., Astel, A., Wolanin, A., & Małek, S. (2011b). Spatiotemporal dynamics of spring and stream water chemistry in a high-mountain area. *Environmental Pollution*, *159*(5), 1048–1057. https://doi.org/10.1016/j.envpol.2010.11.021

Zhi, W., Li, L., Dong, W., Brown, W., Kaye, J., Steefel, C., & Williams, K. H. (2019). Distinct Source Water Chemistry Shapes Contrasting Concentration-Discharge Patterns. *Water Resources Research*, *55*(5), 4233–4251. https://doi.org/10.1029/2018WR024257

Zuecco, G., Penna, D., & Borga, M. (2018). Runoff generation in mountain catchments: Long-term hydrological monitoring in the Rio Vauz Catchment, Italy. *Cuadernos de Investigación Geográfica*, *44*(2), Article 2. https://doi.org/10.18172/cig.3327

Geologic features (e.g., fractures and alluvial fans) can play an important role in the locations and volumes of groundwater discharge and degree of groundwater-surface water (GW-SW) interactions. However, the role of these features in controlling GW-SW dynamics and streamflow generation processes are not well constrained. GW-SW interactions and streamflow generation processes are further complicated by variability in precipitation inputs from summer and fall monsoon rains, as well as declines in snowpack and changing melt dynamics driven by warming temperatures. Using high spatial and temporal resolution radon and water stable isotope sampling and a 1D groundwater flux model, we evaluated how groundwater contributions and GW-SW interactions varied along a stream reach impacted by fractures (fractured-zone) and below the fractured hillslope (non-fractured zone) in Coal Creek, a Colorado River headwater stream affected by summer monsoons. During early summer, groundwater contributions from the

fractured zone dominated, but declined throughout the summer. Groundwater contributions from the non-fractured zone were constant throughout the summer and became proportionally more important later in the summer. We hypothesize that groundwater in the non-fractured zone is dominantly sourced from a high-storage alluvial fan at the base of a tributary that is connected to Coal Creek throughout the summer and provides consistent groundwater influx. Water isotope data revealed that Coal Creek responds quickly to incoming precipitation early in the summer, and summer precipitation becomes more important for streamflow generation later in the summer. We quantified the change in catchment dynamic storage and found it negatively related to stream water isotope values, and positively related to modeled groundwater discharge and the ratio of fractured zone to non-fractured zone groundwater. We interpret these relationships as declining hydrologic connectivity throughout the summer leading to late summer streamflow supported predominantly by shallow flow paths, with variable response to drying from geologic features based on their storage. As groundwater becomes more important for sustaining summer flows, quantifying local geologic controls on groundwater inputs and their response to variable moisture conditions may become critical for accurate predictions of streamflow.

1. Hydrologic connectivity shifts from high to low throughout the summer.
2. Shallow flow paths are important for late summer streamflow generation.
3. Spatial origin of groundwater discharge varies with hydrologic connectivity.
4. Dynamic storage explains variability in groundwater flux and stream water origin.